SEISMIC RESPONSE OF STEEL BEAMS COUPLING CONCRETE WALLS

by

KENT A. HARRIES

May 1992

Department of Civil Engineering and Applied Mechanics
McGill University
Montreal, Canada

A thesis submitted to the Faculty of Graduate Studies and Research in partial fulfilment of the requirements for the degree of Master of Engineering

Abstract

Ductile coupled flexural walls are critical lateral load resisting systems of many structures. The coupling beams of these structures must exhibit excellent ductility and energy absorption ability. To achieve better ductility and energy absorption than previously possible, the use of steel link beams with their ends embedded in the reinforced concrete walls is proposed. Preliminary experimental results are reported for two full-scale reversed cyclic loading tests of portions of ductile flexural walls coupled with steel link beams. The excellent performance, together with the ease of construction, demonstrate the feasibility of this alternative form of construction. In order to ensure ductile response, design and detailing guidelines for both the clear span and embedded portions of the link beams and the reinforced concrete embedment region are presented. An assessment, based on comparisons with other structural systems, of this novel type of construction is presented.

Résumé

Une ossature composée de murs de flexion et de linteaux est fréquemment rencontrée. Les linteaux doivent démontrer une excellente ductilité et absorber beaucoup d'énergie. L'emploi de linteaux en acier de charpente encastrés dans les murs de béton armé est proposé afin d'améliorer la ductilité et l'absorption d'énergie. Les résultats d'études préliminaires sont présentés pour deux spécimens en de contreventement grandeur réelle formés de trumeaux et de linteaux en acier de charpente soumis à des charges cycliques renversées. L'excellent comportement de ce système lors d'un séisme et sa construction simple assure le succès de ce nouveau genre d'ossature ductile. Afin d'assurer un comportement ductile, les procédures de conception et de détail de la portée libre et des portions encastrées des linteaux, ainsi que la région d'encastrement des murs en béton armé, sont présentées Une comparaison avec d'autres systèmes de contreventement, permet d'évaluer l'efficacité de ce nouveau type de construction.

Acknowledgements

The author would like to gratefully acknowledge Professors D. Mitchell and R.G. Redwood for their encouragement and guidance on this programme. Furthermore, the author would like to thank Dr. W.D. Cook for his encouragement and support; Ron Sheppard and John Bartczak for their invaluable work in helping to prepare the specimens and Jamie Mitchell, Andrew Griezic and Albert Wallrap for helping to test the specimens.

The financial support of the Natural Sciences and Engineering Research Council of Canada is gratefully acknowledged.

Table of Contents

List of Figures

List of Tables

List of Symbols

A_1, A_2	area of single wall in coupled system (mm^2)
A_b	cross sectional area of link beam (mm^2)
A_s	area of link beam stiffener (mm^2)
A_w	area of link beam web (mm^2)
b	width of link beam flange (mm)
b'	effective width of compression block at link beam flange (mm)
c	depth of concrete cover (mm)
E	Young's modulus of material (MPa)
e	lever arm of load applied to embedment (mm)
f	shape factor for shear stress distribution (laminar analysis)
f_c'	compressive strength of concrete (MPa)
f_{sp}	splitting strength of concrete (MPa)
F_u	ultimate strength of steel (MPa)
F_y	yield strength of steel (MPa)
h	height of link beam (mm)
h_w	height embedment web (mm)
I_1, I_2	moment of inertia of single wall in coupled system (mm^4)
I_b	moment if inertia of link beam (mm^4)
I_o	moment of inertia of entire coupled wall system (mm^4)
I_x	reduced moment of inertia of link beam allowing for shear deflection (mm^4)
L	clearspan of link beam (mm)
L_{cr}	maximum unsupported length of link beam (mm)
L_e	required length of embedment (mm)
L_{eff}	effective clearspan of link beam (mm)
M_f	factored moment (kN•m)
M_r	factored moment resistance (kN•m)
P	point load applied to top of structure (kN)
R	force modification factor (NBCC, 1990)
r	radius of gyration (mm)
t	thickness of link beam flange (mm)
t_w	thickness of embedment web (mm)
T_x	axial force in wall at level x (kN)
V	equivalent seismic base shear (NBCC, 1990) (kN)
V_c	shear resistance of embedment (kN)
V_f	factored shear (kN)
V_r	factored shear resistance (kN)
W_f	uniformly distributed lateral load on structure (kN/m)
w	thickness (width) of link beam web (mm)
W	linearly distributed lateral load on structure (kN/m)
x	distance measured from top of structure (laminar analysis) (m)
Z	section modulus (mm)
β	equivalent elastic damping coefficient
γ_p	rotation of link beam in eccentrically braced frame, from Engelhardt and Popov (1989)
δ_y	displacement at yield (mm)
ϕ	resistance factor for steel (0.90)
ϕ_c	resistance factor for concrete (0.60)
ϕ_s	resistance factor for reinforcing steel (0.85)
μ	ductility

Chapter 1
Introduction

1.1 Introduction

The Supplement to the 1990 National Building Code of Canada (NBCC Supplement, 1990) states that an acceptable level of public safety can be achieved if structures are designed such that they are "able to resist moderate earthquakes without significant damage and major earthquakes without collapse". The 1990 NBCC specifies an equivalent seismic base shear, V, which is calculated from the following expression:

$$V = \left(\frac{V_e}{R}\right)U$$

where U = a calibration factor, taken as 0.6,
R = force modification factor, and

V_e = equivalent *elastic* base shear, given as: $V_e = vSIFW$ with:

v = zonal velocity ratio,
S = seismic response factor,
I = importance factor,
F = foundation factor, and
W = the weight of the structure

The force modification factor, R, reflects the ability of a structure to dissipate energy through inelastic behaviour. In the 1990 NBCC the values of R vary from 1.0, for unreinforced masonry, to 4.0, for ductile moment resisting steel or concrete frame structures.

1.1.1 Ductile Flexural Walls

The 1990 NBCC, recognises that ductile flexural walls are capable of exhibiting significant inelastic deformations without loss of strength and specifies a force modification factor, R, of 3.5.

Ductile flexural walls are designed in accordance with the requirements of CSA Standard CAN3-A23.3-M84, Design of Concrete Structures for Buildings (CSA, 1984). The Special Provisions for Seismic Design, Clause 21, state that ductile flexural walls must be designed to resist the forces and dissipate energy through flexural yielding at one or more plastic hinges. This is achieved by designing the walls to yield in flexure without local instability or shear failures. Furthermore, stringent requirements are placed on the flexural ductility of the walls, the detailing of the wall reinforcement and the minimum amounts of reinforcement in the walls.

Walls with a regular pattern of openings are called coupled walls. They are composed of two or more walls linked with coupling beams above and below each opening. Ductile coupled flexural walls are designed such that the coupling beams are the primary energy dissipating elements. This is achieved in the CSA A23.3 Standard by first designing the coupling beams such that shear failures are avoided and by detailing the coupling beams to enable full yielding of the main reinforcement. The Standard requires that ductile coupling beams be reinforced with well confined diagonal reinforcement or, when the shear stress is low and the span-to-depth ratio is relatively high, then the beams may be designed and detailed as ductile flexural beams. In order to ensure that the beams are capable of dissipating significant amounts of energy, the walls are designed to resist the forces corresponding to hinging in all of the beams. Therefore a ductile coupled flexural wall system is able to dissipate significant amounts of energy by hinging of the coupling beams without significant inelastic action occurring in the walls.

1.2 Analysis of Coupled Wall Systems

It is clear from their function that the coupling beams in a coupled wall system are the critical energy absorbing elements and thus their strength will dictate the required strengths of the walls. The first step in the design is to determine the forces in the coupling beams due to lateral loading.

The equivalent lamina method and the equivalent frame method are the most common methods of analysing coupled shear walls. These two methods of analysis are discussed below.

1.2.1 Equivalent Lamina Analysis of Coupled Flexural Walls

The determination of the forces in the coupling beams of a coupled flexural wall system is highly statically indeterminate. In order to analyse the system, the link beams are replaced with an equivalent elastic lamina as shown in Fig. 1.1. The forces in the coupling beams can be

determined from a single, second order differential equation when the following assumptions are made:

i) the floor heights are uniform, so that the link beams are equally spaced,

ii) the link beams all have the same properties, with the exception of the topmost one, whose stiffness is assumed to be one half the stiffness of the other beams,

iii) the properties of the walls do not vary with height,

iv) the axial deformations of the link beams are neglected,

v) the shear deformations of the walls are neglected,

vi) the stiffnesses of the walls are assumed to be much greater than that of the link beams, consequently the slopes of the walls are the same at any level, implying that the points of contraflexure in the link beams are at their midspans, and

vii) the lateral load can be expressed as a continuous function over the height of the structure.

The differential equation, based on conditions of equilibrium and compatibility was expressed by Rosman (1964) as the relationship between the external moment, M_e, the axial force in the wall, T_x, and the laminar shear force, q_x, at any level of the wall, as:

$$\frac{1}{EI_e}\int_x^H M_e\,dx - \frac{l^2}{EI_e}\int_x^H T_x\,dx - \frac{1}{E}\left(\frac{1}{A_1} + \frac{1}{A_2}\right)\int_x^H T_x\,dx - \frac{hl_b^3}{12EI_x}q_x = 0 \qquad (1.1)$$

with

$$I_x = \frac{I_b}{1 + \dfrac{12EI_bf}{GA_bl_b^2}} \qquad (1.2)$$

where

x = the distance measured from the top of the structure,
I_x = the reduced moment of inertia of the coupling beam allowing for shear deformation,
A_b = cross-sectional area of the beam,
I_b = moment of inertia of the beam,
f = shape factor to account for the shear stress distribution in link beam, and
I_e, A_1, A_2, l, l_b are geometric properties of the system as defined in Fig. 1.1.

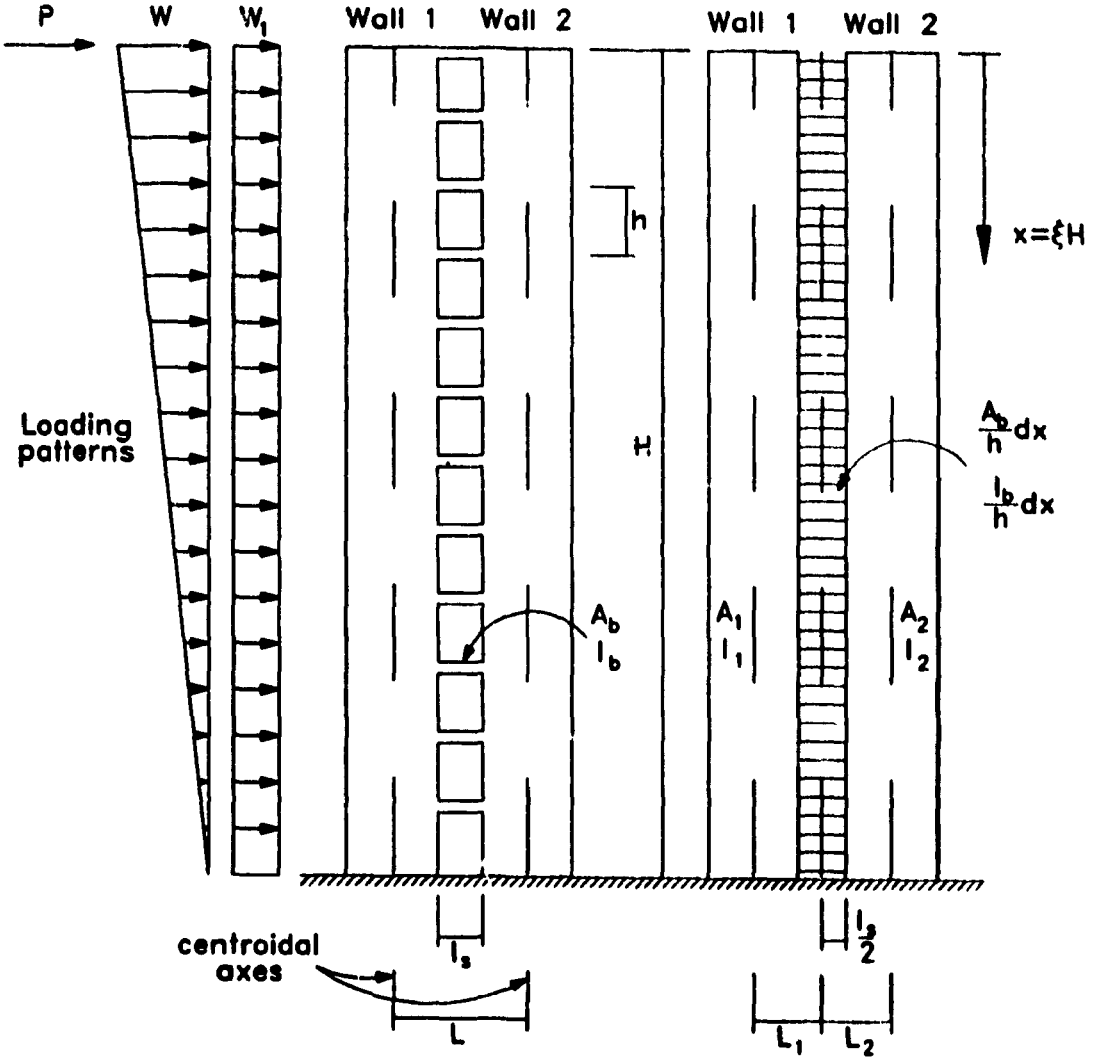

Figure 1.1 Equivalent lamina representation of coupled shear walls (adapted from Stafford-Smith and Coull, 1991)

Combining the common terms and differentiating with respect to x, the differential equation for the axial force in the walls is obtained as:

$$\frac{d^2T_x}{dx^2} - \alpha^2 T_x = -\gamma M_o \qquad (1.3)$$

where T_x is the axial force in the wall at x and;

$$\alpha^2 = \left(\frac{1}{A_1} + \frac{1}{A_2} + \frac{l^2}{I_o}\right)\left(\frac{12I_x}{hH_o^3}\right) \quad \text{and} \quad \gamma = \frac{12H_x}{I_o H_o^3} \qquad (1.4)$$

Considering the following three loading patterns on the shear wall, as shown in Fig. 1.1:

i) A single point load, P applied to the top of the shear wall,
ii) A linearly distributed load, W acting with maximum intensity at the top of the structure,
iii) A uniformly distributed load, W_1.

The bending moment at any level due to these loads is:

$$M_o = WH\left(\xi^2 - \frac{\xi^3}{3}\right) + PH\xi + W_1H\frac{\xi^2}{2}, \quad \text{where } \xi = \frac{x}{H} \tag{1.5}$$

Considering that each wall has a fully fixed base, the boundary conditions become:

i) when x = 0, T = 0 (i.e., at the top of the structure) and,
ii) when x = H, q = 0, that is dT/dx = 0 (i.e., at the base of the structure)

Substituting these conditions into the differential equation, the axial force, T_x, can be found. Recognising that the axial force is the accumulation of laminar shear, the equation for laminar shear can be written as (Santhakumar, 1974):

$$q(\xi) = \left(\frac{dT(\xi)}{d\xi}\right)\left(\frac{1}{H}\right) \tag{1.6}$$

Defining the following parameters as:

$$\beta = \alpha H, \quad \rho = \frac{P}{W} \text{ and } \quad \rho' = \frac{W_1}{W}$$

and substituting these parameters, together with Equation 1.6, into Equation 1.1 results in the following expression for the laminar shear:

$$q(\xi) = \left(\frac{\gamma WH^2}{\beta^3}\right)\left[\begin{array}{c}(2+\rho')\tanh\beta\cosh\beta\xi + \dfrac{\cosh\beta\xi}{\cosh\beta}\left(\dfrac{2}{\beta} - \beta - \rho'\beta - \rho\beta\right)\cdots \\ -(2+\rho')\sinh\beta\xi + 2\beta\xi - \beta\xi^2 + \beta\rho + \beta\rho'\xi - \dfrac{2}{\beta}\end{array}\right] \tag{1.7}$$

The lateral deflection of the shear wall, at any level, x, can be derived from the general expression:

$$EI_o\frac{d^2y}{dx^2} = M_o - IT_x \tag{1.8}$$

which can be expressed as:

$$y(\xi) = \left(\frac{WH^2}{EI_o}\right)\left\{\begin{array}{l}\frac{1}{60}\left(\frac{\gamma^1}{\alpha^2}-1\right)[\xi^5-5\xi^4+15\xi-11-10\rho(\xi^3-3\xi+2)+\rho'(10\xi-2.5\xi^4-7.5)]\ldots \\ -\frac{\gamma^1}{\alpha^2\beta^4\cosh\beta}\left[\begin{array}{l}(\sinh\beta\xi-\sinh\beta)\left(2\sinh\beta+\frac{2}{\beta}-\beta-\beta\rho-\beta\rho/+\rho/\sinh\beta\right)\ldots \\ -\cosh\beta(2+\rho)(\cosh\beta\xi-\cosh\beta)-\frac{\beta^2\cosh\beta}{3}(\xi^3-3\xi^2\rho'+1.5)\ldots \\ +3(\xi-1)\left(\frac{2}{\beta^2}-\rho\right)+2\end{array}\right]\end{array}\right\} \quad (1.9)$$

1.2.2 Equivalent Frame Method of Modelling Coupled Flexural Walls

While the equivalent lamina analysis is appropriate for uniform flexural walls, it is unable to adequately deal with more complex systems. An equivalent frame analysis (MacLeod, 1966 and Schwaighofer and Microys, 1969), provides a more realistic and more versatile approach for more complex systems.

An equivalent frame model represents each wall with an equivalent 'wide column' located at the centroidal axis of the wall. The axial rigidity, EA, and the flexural rigidity, EI, of each wall is assigned to a column of the equivalent frame. Typically, shear deformations in the walls are neglected since the flexural behaviour will dominate the response of the walls.

The coupling beams are represented by frame elements located at the centroidal axis of each coupling beam. In order to account for shear deformations of the coupling beam, the moment of inertia assigned to each beam member is determined from the relation given by Equation 1.2. Rigid offsets span from the centroidal axes of the walls (equivalent column) to the ends of each coupling beam. These rigid offsets simulate the 'wide column' effect and satisfy the assumption that plane sections in the walls remain plane. The rigid offsets ensure that the correct rotations and vertical displacements are produced at the ends of the coupling beams. Figure 1.2 illustrates the representation of a coupled wall system as an equivalent frame.

The equivalent frame method has the additional advantage that the coupled wall system can be linked with the rest of the structure, enabling the structural interaction to be determined.

The prototype structure presented in Chapter 2 was analysed using both the equivalent lamina and equivalent frame methods and some comparative results are shown in Fig. 2.2.

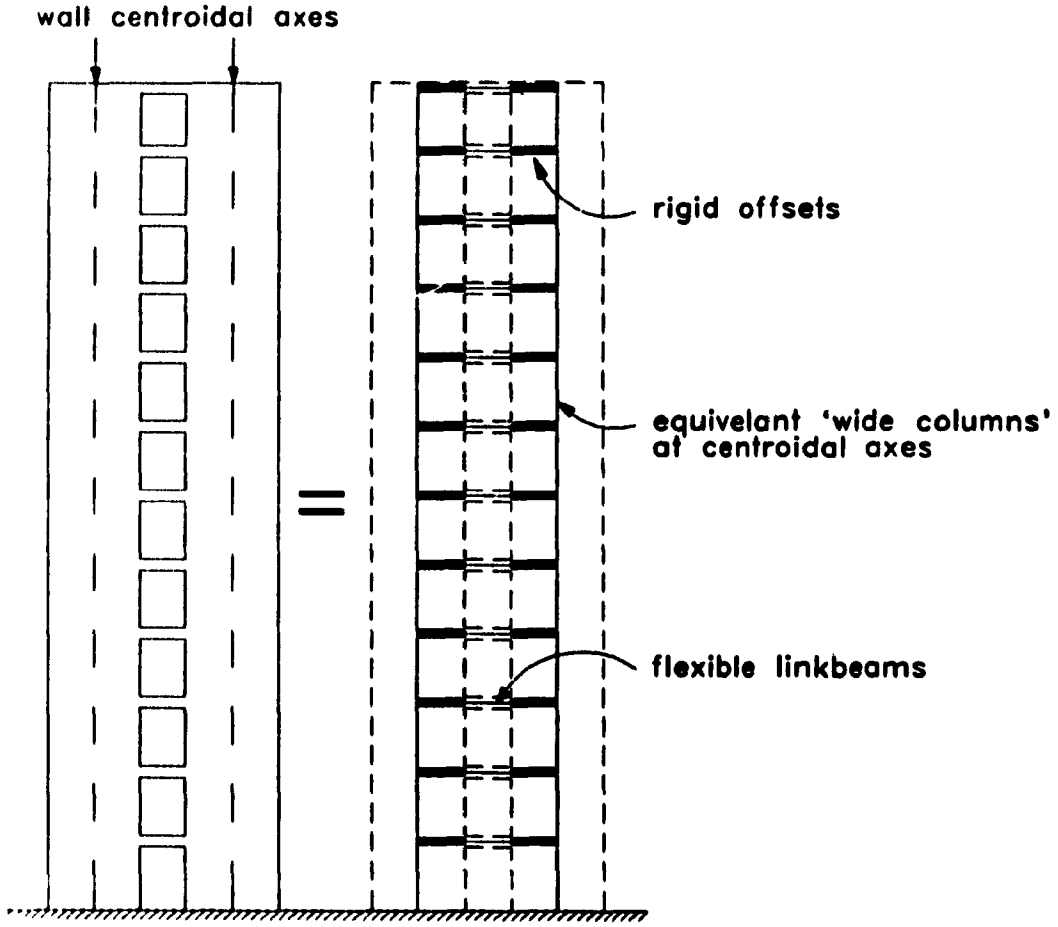

Figure 1.2 Equivalent frame representation of coupled shear walls (adapted from Stafford-Smith and Coull, 1991)

1.3 Previous Research

1.3.1 Tests of Reinforced Concrete Coupling Beams and Coupled Walls

Following the 1964 Alaskan earthquake, (Berg and Stratta, 1964) considerable attention was devoted to improving the response of reinforced concrete coupling beams in coupled wall systems.

Extensive experimental work, under the direction of Paulay at the University of Canterbury, led to the development of design guidelines for reinforced concrete coupling beams. Tests conducted by Paulay (1969 and 1971) led to design guidelines for coupling beams with relatively

large span-to-depth ratios and relatively low shear stress levels. The design philosophy developed for these members avoids brittle shear failures by providing shear resistances large enough to develop flexural hinging in the beams (Park and Paulay, 1975). Conventionally reinforced beams with relatively small span-to-depth ratios and/or high shear stress levels exhibited sliding-shear failures at the wall interfaces (Paulay and Binney, 1974 and Park and Paulay, 1975). Because the sliding-shear plane is perpendicular to the beam span, conventional transverse reinforcement has no effect in controlling this mode of failure.

To prevent sliding-shear failures, Paulay and Binney (1974) introduced the concept of using diagonal reinforcement in the coupling beams (see Fig 1.3). Diagonally reinforced coupling

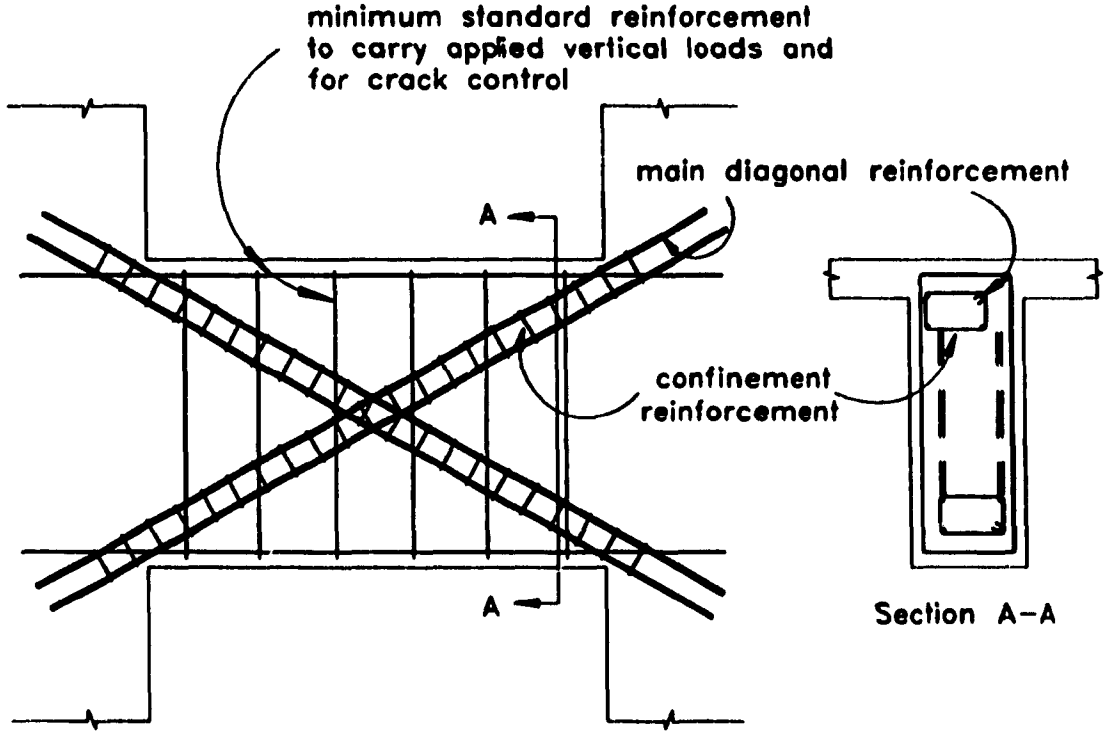

Figure 1.3 Diagonal reinforcement of coupling beams

beams offered improved ductility and energy absorption over conventionally reinforced coupling beams. Santhakumar and Paulay (1974) conducted quarter-scale model tests on seven storey coupled walls having coupling beams with a span-to-depth ratio of 1.25. These tests confirmed the superior performance of diagonally reinforced coupling beams, with the attainment of larger displacement ductilities and energy absorption compared with conventionally reinforced coupling

beams. With the diagonally reinforced beams, displacement ductilities of the wall system of 8 to 13 were achieved without loss of strength.

The University of Canterbury research forms the basis for the design criteria for coupling beams in ductile coupled flexural walls given by the CSA A23.3 Standard.

Research conducted at the Portland Cement Association (PCA) examined the response of relatively slender coupling beams, having span to depth ratios of 2.5 and 5 (Shiu, et al, 1978). These tests confirmed the improved behaviour of diagonally reinforced beams over conventionally reinforced beams (see Fig. 1.4). However these tests demonstrated that for larger span to depth ratios the diagonal reinforcement is not as efficient due to its lower inclination. These tests also confirmed the need for closely spaced hoops or spiral reinforcement confining the diagonal bars, both in the coupling beam and along their wall embedments. If adequate confinement is not provided, then buckling of the diagonal bars may severely affect the response.

1.3.2 Steel Link Beams in Eccentrically Braced Frames

Analogous to coupling beams in reinforced concrete coupled wall systems, steel link beams in eccentrically braced frames (EBFs) serve as the primary ductile energy absorbing elements. Recent research has shown that steel link beams in eccentrically braced frames can be detailed to provide excellent ductility and energy dissipating characteristics.

A number of research programmes, under the direction of Popov, have been carried out at the University of California, Berkeley (Malley and Popov, 1983a and 1983b, Roeder and Popov, 1978 and Kasai and Popov, 1986). The results of these programs have led to design recommendations for achieving large ductility and energy absorption characteristics from link beams. Engelhardt and Popov (1989) provide an excellent summary of design and detailing considerations for achieving ductile response from steel link beams of varying spans.

This research clearly indicates the superior hysteretic response of steel beams particularly when they are designed to yield in shear while remaining elastic in flexure. Malley and Popov (1983b) demonstrate the necessity for detailing link beams to control web and/or flange instability with the provision of stiffeners.

This work has led to the design and detailing requirements for link beams in EBFs that form the basis of the provisions of Appendix D in the Canadian Steel Design Standard, CAN/CSA S-16.1-M89 (CSA, 1989).

1.3.3 Reinforced Concrete Coupling Beams Containing Encased Steel Members

Although no experimental research has been published on the use of steel beams to connect reinforced concrete walls, there have been some investigations carried out on reinforced

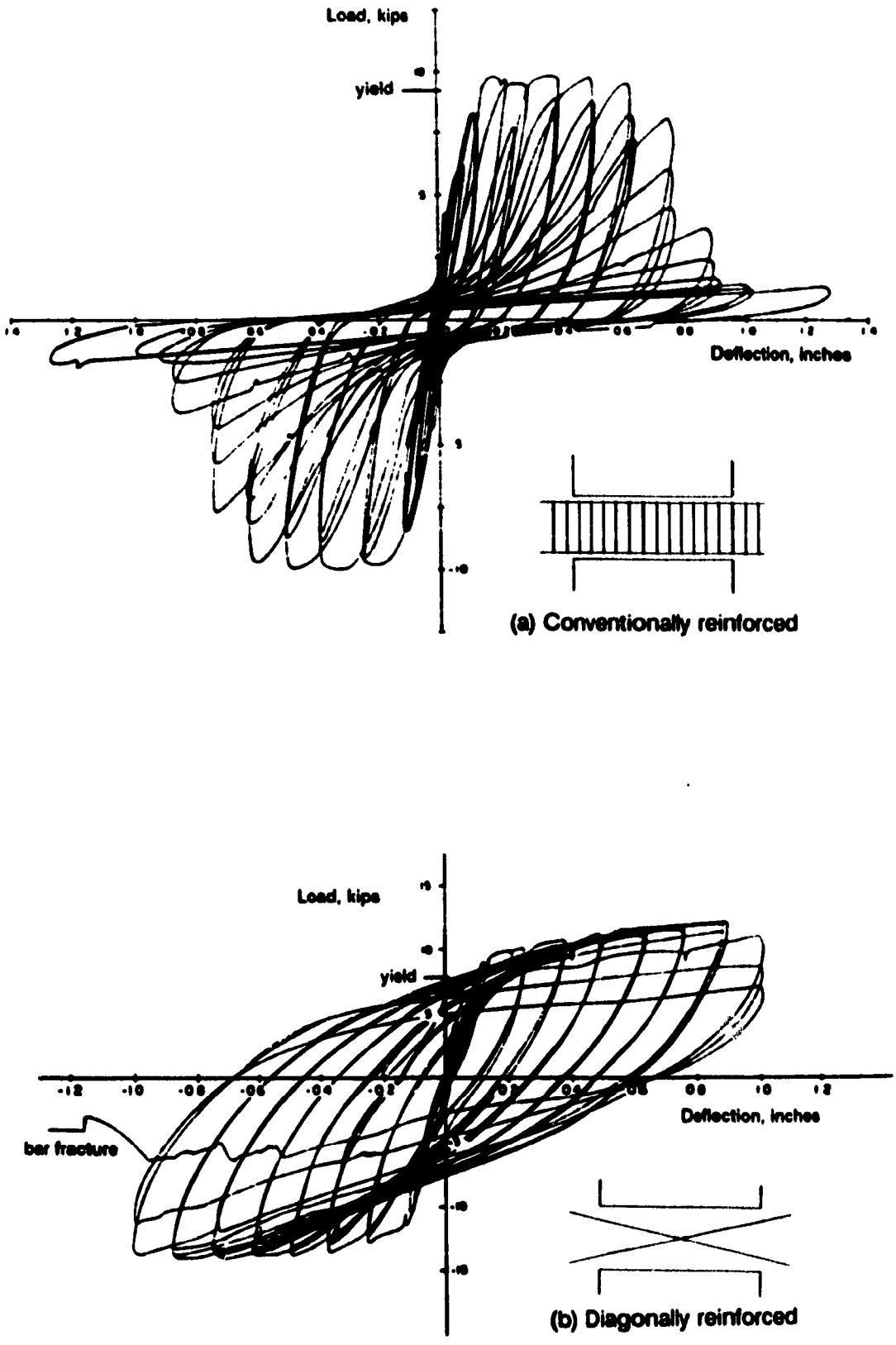

Figure 1.4 Load versus deflection response for conventionally reinforced (top) and diagonally reinforced (bottom) coupling beams with span-to-depth ratios of 2.5 (from Shiu, et al, 1978)

concrete coupling beams containing structural steel members. It is interesting to note that many older reinforced concrete coupled wall systems have steel members encased in the coupling beams. These steel members often served as erection steel and were not typically accounted for in design.

Paparoni (1972) reported on a study of a reinforced concrete coupling beam containing an encased structural "I" section tested at the Laboratorio Nacional de Engenharia Civil in Lisbon. This study investigated the reversed cyclic loading response of a 130 mm wide by 230 mm deep reinforced concrete coupling beam spanning 450 mm containing conventional longitudinal and transverse reinforcement and a 140 mm deep structural "I" section. The test specimen was a model of coupling beams in the Parque Central buildings in Caracas Venezuela. The testing programme also investigated the reversed cyclic loading response of coupling beams reinforced with a combination of longitudinal and inclined reinforcing bars together with closed stirrups. The details of the special inclined reinforcement for these coupling beams, having a span-to-depth ratio of 2, were different than those suggested by Paulay. The results of these tests suggested that reinforced coupling beams having encased structural steel members and those reinforced with the special inclined reinforcement exhibited ductilities and energy absorption characteristics between those of conventionally reinforced and diagonally reinforced coupling beams.

Research conducted at McGill University by Mitchell and Cook (1989) investigated the reversed cyclic loading response of a reinforced concrete coupling beam containing a structural steel channel. The encased channel is representative of erection steel used in some older structures. The 280 mm wide by 610 mm deep coupling beam spanning 1525 mm contained longitudinal reinforcing bars and closely spaced closed stirrups as well as a 150 mm deep structural channel. The results of this test showed some improvement in ductility and hysteretic behaviour over conventionally reinforced link beams.

Another research programme which involved composite link beams was carried out at the University of Dundee by Subedi (1989). This programme involved replacing conventional shear reinforcement with encased steel plates. The results from this preliminary testing programme indicated that premature shear failure may result if the plate has inadequate anchorage to the concrete. Several different methods were investigated in an attempt to provide horizontal shear resistance between the encased steel plate and the longitudinal reinforcing bars. The specimens of this test series were subjected to monotonic loading only and it is doubtful if the details proposed would perform well under reversed cyclic loading.

1.3.4. Embedded Connections of Structural Steel Members in Reinforced Concrete

Structural steel members with their ends embedded in concrete, serving as haunches or brackets, have been used to provide connections for many years in precast and cast-in-place construction. Marcakis and Mitchell (1980) investigated the response of different types of structural steel members embedded in reinforced concrete and proposed a design procedure for determining the embedment strength of such connections. This approach forms the basis of current design recommendations for these type of connections (PCI, 1985 and CPCI, 1987). The tests demonstrated that the embedded connection can be designed to develop the full capacity of the embedded structural steel member.

1.4 Objectives of Research Programme

Several researchers have investigated novel approaches for improving the ductility and energy absorption of reinforced concrete coupling beams. For span-to-depth ratios less than about 2, specially detailed diagonal reinforcement (e.g., Paulay and Binney, 1974) has been shown to significantly improve the reversed cyclic loading response. Structural steel members, fully encased in reinforced concrete coupling beams (e.g., Paparoni, 1972 and Mitchell and Cook, 1989) have resulted in slightly improved responses over conventionally reinforced coupling beams. The objective of this research programme is to investigate the feasibility of using structural steel members, having their ends embedded in the walls, to replace reinforced concrete coupling beams.

The use of steel coupling beams to connect reinforced concrete walls has the following potential advantages:

i. Properly designed and detailed steel coupling beams can exhibit excellent ductility and energy absorption.

ii. The prefabrication of steel coupling beams provides improved quality control and eliminates a considerable amount of on-site labour.

iii. Formwork can be significantly simplified.

The specific objectives of this research programme are:

i. To test full-scale specimens under reversed cyclic loading to determine the hysteretic response of structural steel link beams having their ends embedded in reinforced concrete walls.

ii. To attempt to achieve a reversed cyclic loading response similar to that exhibited by steel link beams in eccentrically braced frames.

iii. To investigate factors influencing the reversed cyclic loading response of the link beam over its clear span and along its embedments.

iv. To investigate factors influencing the reversed cyclic loading response of the reinforced concrete embedment regions.

v. To develop design and detailing guidelines to enable large ductilities and energy absorbing capabilities to be achieved in steel link beams used to couple reinforced concrete flexural walls.

Chapter 2
Prototype Structure

2.1 Introduction

The analysis of the prototype structure was carried out using the 1990 National Building Code of Canada (NBCC) to determine the lateral design forces. In order to achieve the desired ductility, the steel link beam was designed in accordance with Clause 27, Seismic Design Requirements, and Appendix D, Seismic Design Requirements for Eccentrically Braced Frames, of CAN/CSA S16.1-M89. Design of the ductile concrete walls was in accordance with Clause 21, Special Provisions for Seismic Design, of CAN/CSA A23.3-M84. The reinforced concrete region surrounding the link beam embedment had to be carefully designed and detailed so that the desired level of ductility could be achieved in the link beam.

2.2 Prototype Structure

The prototype structure is a twelve storey reinforced concrete flat plate structure having a centrally located core. The structure, shown in Fig. 2.1, consists of 5 - 6 m bays in the North-South direction and 7 - 6 m bays in the East-West direction. There is a 1.5 m cantilever slab around the periphery of the structure. The storey heights are 3.65 m except the first storey which has a height of 4.85 m. The structure has 600 mm square columns supporting a 200 mm flat plate floor slab system.

The elevator core is 6 m by 9 m and is designed as a ductile flexural wall in both directions. The walls are 300 mm thick. The 9 m long East-West walls are a coupled system consisting of two 3.9 m walls linked by a 1.2 m long coupling beam located at each floor level. The 6 m long East-West walls are flexural walls without openings.

The prototype structure is located in Vancouver. The core was designed as ductile flexural walls to carry 100 percent of the lateral loads in each principal direction. The corresponding seismic force modification factor, R, is 3.5 (NBCC 1990).

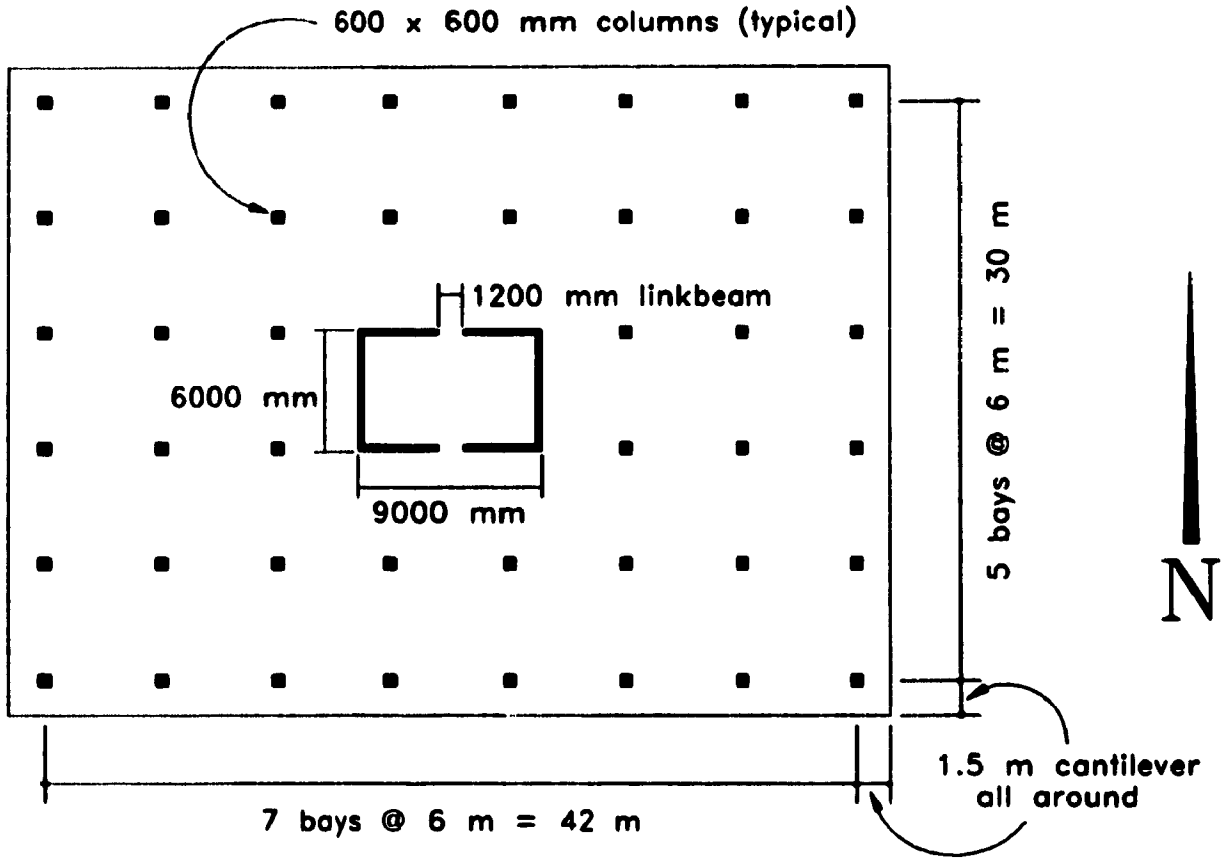

Figure 2.1 Prototype structure

2.2.1 Material Properties

The following specified values were used for the design of this structure:

Concrete: normal density concrete with $f_c' = 35$ MPa

Reinforcing Steel: $f_y = 400$ MPa

Link beam Steel: $F_y = 300$ MPa

2.2.2 Loading on Structure

The following National Building Code of Canada (NBCC) loading criteria were used in the analysis of the structure:

Floor live load:	2.4 kN/m^2 on office bays 4.8 kN/m^2 on corridor bays
Floor dead load:	1.5 kN/m^2 partitions and mechanical
Roof load:	2.2 kN/m^2 full snow load 0.5 kN/m^2 insulation 1.6 kN/m^2 mechanical services over two bays only
Wind loading:	1.72 kN/m^2 net lateral pressure on all storeys
Seismic loading:	Period estimated from equation $T = \frac{0.09 h_n}{\sqrt{D_s}}$ from NBCC Clause 4.1.9.1.(7). T = 1.35 in the East-West direction R=3.5 for ductile flexural wall, from NBCC 4.1.9.1.(8). zonal velocity ratio, v=0.2 for Vancouver.

The base shear due to seismic loading, defined by NBCC Clauses 4.1.9.1.(4) and (5), was 5829 kN in the East-West direction. The concentrated load at the top of the structure, defined by Clause 4.1.9.1.(13)(a), F_t, was 551 kN. The remaining seismic lateral load was distributed over the height of the structure in accordance with the formula given in Clause 4.1.9.1.(13)(a).

The factored base shear due to lateral wind load, determined according to NBCC Clause 4.1.8.1, was found to be 3483 kN in the East-West direction and 4876 kN in the North-South direction, represented by uniformly distributed lateral loads of 77.4 and 108.4 kN per metre of height, respectively. All lateral loads were considered to be resisted by the core alone. The coupled wall system in the East-West direction was modelled as two C-shaped walls interconnected by coupling beams (see Fig. 2.1). Table 2.1 summarises the values of the factored design shears in the link beams obtained from the equivalent lamina analyses. The storey drifts from seismic loads given in Table 2.1, have been multiplied by R in order to account for the inelastic deformations. In the preliminary design torsional effects were neglected. Figure 2.2 illustrates the values for the shear forces in the coupling beams for both the equivalent lamina and the equivalent frame analyses. As can be seen, the shapes of the distributions of shears in the beams are similar, with the equivalent frame method giving lower shears near the base of the structure.

Storey	NBCC Seismic Loading Conditions			NBCC Wind Loading Conditions		
	Link beam Shear (kN)	Horizontal Deflection (mm)	Storey Drift x R (mm)	Link beam Shear (kN)	Horizontal Deflection (mm)	Storey Drift (mm)
12	125	263		99	46	
11	251	243	70	101	40	5.7
10	254	223	71	106	35	5.6
9	258	202	72	111	29	5.5
8	259	181	73	116	24	5.4
7	258	160	75	120	19	5.2
6	251	138	76	124	14	5.0
5	237	116	77	126	9	4.6
4	216	93	78	125	5	4.1
3	186	71	78	121	2	3.3
2	145	49	77	112	-1	2.3
1	92	27	75	99	-2	0.9
ground		0	95		0	-1.6
maximum acceptable storey drift for seismic load, $0.02h_s$ = 97 mm for ground storey and 73 mm for other storeys.						

Table 2.1 Summary of link beam shears and horizontal wall deflections from preliminary analyses

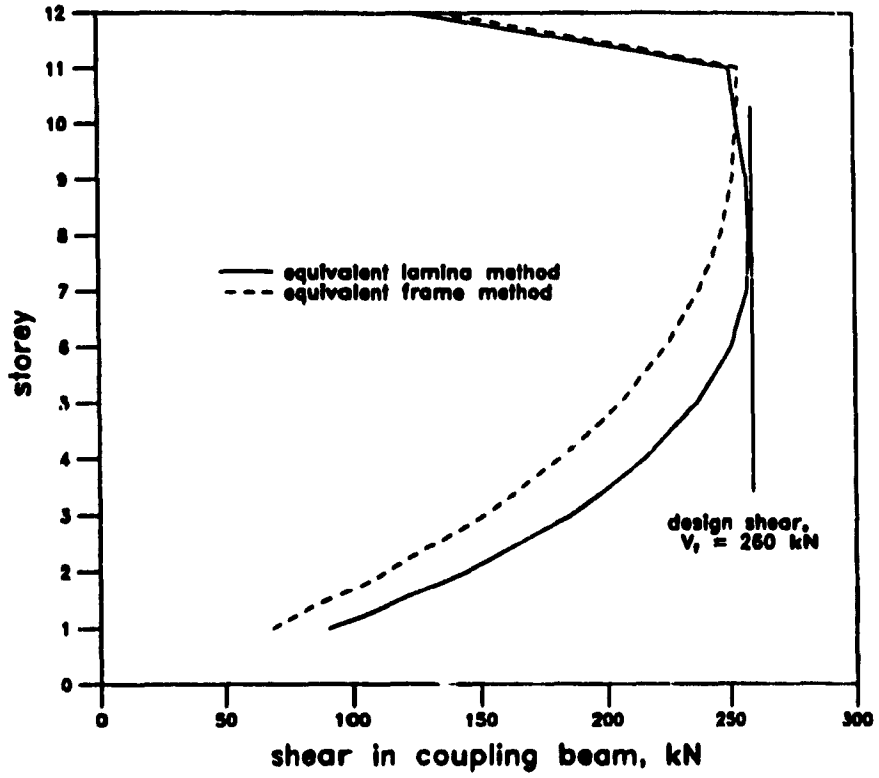

Figure 2.2 Shears in coupling beams determined from equivalent lamina and equivalent frame analyses

Chapter 3
Specimen Design and Detailing

3.1 Design of the Steel Link Beam and Embedment Region

3.1.1 Design of the Exposed Span of the Link Beam

The steel link beam was designed in accordance with CAN/CSA S16.1-M89 Clause 27, Seismic Design Requirements. Appendix D, Seismic Design Requirements for Eccentrically Braced Frames, provides design and detailing requirements for link beams in eccentrically braced frames, the principles of which are directly applicable to the design of a ductile steel coupling beam.

Since the coupling beam in a ductile coupled wall system is the critical element, it must respond in a ductile manner and exhibit significant energy absorbing characteristics. Unlike reinforced concrete coupling beams, which are designed to avoid shear failures and to develop flexural hinges, steel coupling beams are more ductile and are able to dissipate significantly larger amounts of energy if they are designed and detailed to yield in shear. Since the shear-to-moment ratio is large in typical short-span link beams, this "shear critical" design criterion is attainable.

In design of such a link beam, the primary requirement is to ensure that the ultimate shear capacity of the link beam will be reached while the beam remains elastic in flexure. This requirement will ensure that the maximum amount of energy will be dissipated when the link beam begins to exhibit plastic behaviour.

The steps for designing and detailing the exposed portion of the link beam are as follows:

Step 1: Determine the web area, A_w, required to resist the factored shear, V_f, from the following expression used for plastic design for the factored shear resistance, V_r:

$$V_r = 0.55 A_w F_y \qquad (3.1)$$

where: F_y = specified minimum yield stress.

Step 2: Choose the height, h, and the width, w, of the web to give the required A_w and to satisfy the following limits for a Class 1 section in order to avoid local buckling of the web:

$$\frac{h}{w} \leq \frac{1100}{\sqrt{F_y}} \qquad (3.2)$$

Step 3: Determine the required section modulus, Z, such that the section has a moment resistance, M_r, greater than or equal to the moment corresponding to the development of strain hardening in shear:

$$Z = \frac{M}{\phi F_y} \qquad (3.3)$$

where: $M = \frac{L}{2} \times 1.27 V_r$,

L = the clear span of the link beam,
ϕ = material resistance factor, typically taken as 0.90, and
the factor 1.27 accounts for the development of strain hardening.

Step 4: In choosing a section to give the required Z, the contribution of the web should be ignored since it will be yielding in shear. Choose the flange dimensions such that the width of the flange, b, and the thickness of the flange, t, satisfy the limits for a Class 1 section, in order to avoid local buckling of the flange:

$$\frac{b}{2t} \leq \frac{145}{\sqrt{F_y}} \qquad (3.4)$$

Step 5: In order to control out of plane buckling, the maximum unsupported length of the link beam, L_{cr}, is given as:

$$L_{cr} = \frac{980 r_y}{\sqrt{F_y}} \qquad (3.5)$$

where: r_y = the radius of gyration of the section.

Step 6: Provide full depth stiffeners at the faces of the concrete walls. These stiffeners must have a combined width of at least b - 2w, although providing stiffeners wide enough to be flush with the link beam flange tips would simplify the formwork details. The stiffeners must have a thickness no less than 0.75w nor 10 mm.

Step 7: Provide full depth intermediate stiffeners at a spacing no greater than 38w - 0.2d. If the depth of the link beam is less than 650 mm, intermediate stiffeners may be placed on only one side of the web. In this case the width of the stiffeners must be greater than 0.5b - w and the thickness must be greater than 10 mm. If

stiffeners are provided on both sides of the web, the limits given in step 6 for width and thickness apply.

Step 8: Design the fillet welds connecting the stiffeners (Area = A_s) to the link beam web in order to develop a stiffener force of A_sF_y. The fillet weld connecting the stiffener to the link beam flanges must be designed to develop a stiffener force of $0.25A_sF_y$.

Step 9: If the beam is a built-up section, the design of the flange-to-web welds must be carried out in accordance with Clause 13.13.

Since the design of a ductile coupled wall system is based on capacity design principles, it must be recognised that any excess strength provided in the link beams will require additional resistances throughout the concrete walls in order to achieve the desired hierarchy of yielding.

3.1.2 Design of the Reinforced Concrete Embedment Region

Since the link beam is required to undergo significant inelastic deformation its embedment must be capable of developing the capacity of the link beam.

The design of the concrete embedment of the link beam is modelled after the design of steel haunches in concrete members developed by Marcakis and Mitchell (1980) and recommended by the design handbooks of the Prestressed Concrete Institute (1985) and the Canadian Prestressed Concrete Institute (1987). This approach assumes rigid body rotation of the embedded section in calculating the applied concrete stresses over the length of the embedment. Figure 3.1 illustrates the assumed strain distributions and the equivalent rectangular stress blocks over the embedment length.

The steps for designing the embedment of the link beam are summarised as follows:

Step 10: Determine the effective width, b', of the concrete compression block. This width is defined as the width of the confined wall region measured to the outside of the confinement steel but should not exceed 2.5 times the bearing width, b. (see Figure 3.1)

Step 11: Determine the required length of embedment, L_e, such that the factored shear resistance, V_e, of the embedment is greater than the shear capacity of the exposed link beam, including the effects of strain hardening. This shear capacity is taken as $1.27V_r$. Hence, the minimum value of L_e can be determined from the following relationship:

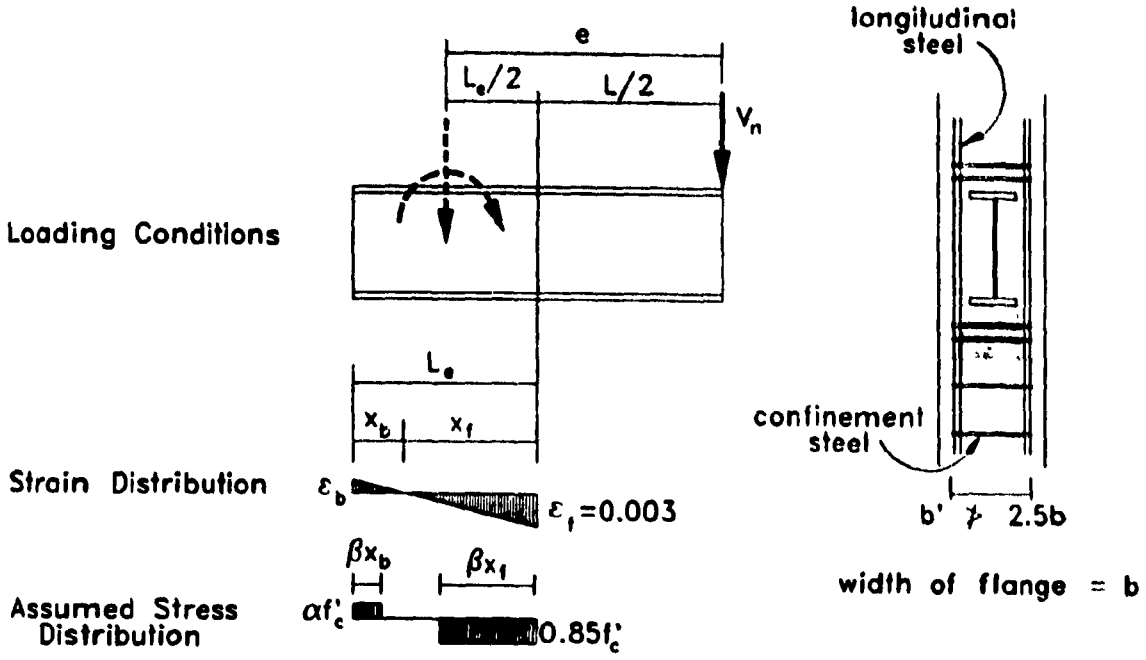

Figure 3.1 Assumed strain and stress distribution over the embedment (adapted from Marcakis and Mitchell, 1980)

$$1.27V_f \le V_c = \frac{0.85\phi_c f'_c b' L_e}{1 + \frac{3.6e}{L_e}} \qquad (3.6)$$

where: e = the eccentricity of resultant shear loads from the centre of the embedment (i.e., $e = \frac{L}{2} + \frac{L_e}{2}$), and

f'_c = the compressive strength of concrete.

thus the minimum length of embedment is found from the quadratic solution to Equation 3.6 as:

$$L_e = \frac{1}{2}\left[\frac{3.56V_f}{0.85f'_c b'} + \sqrt{\left(\frac{3.56V_f}{0.85f'_c b'}\right)^2 + \frac{9.14V_f L}{0.85f'_c b'}}\right] \qquad (3.7)$$

The design procedure for embedments described above was developed for monotonic loading. For reversed cyclic loading additional design considerations are required. Upon reversal of the loading the gap created at the link beam flange-concrete interface will first have to be closed before significant resistance can be realised. If the gap becomes too large upon cycling then an undesirable hysteresis response of the connection region will result. In order to control the gap, it is necessary to provide sufficient vertical reinforcing bars crossing the link beam-concrete interface (see Fig 3.2). The amount of steel required can be determined as follows:

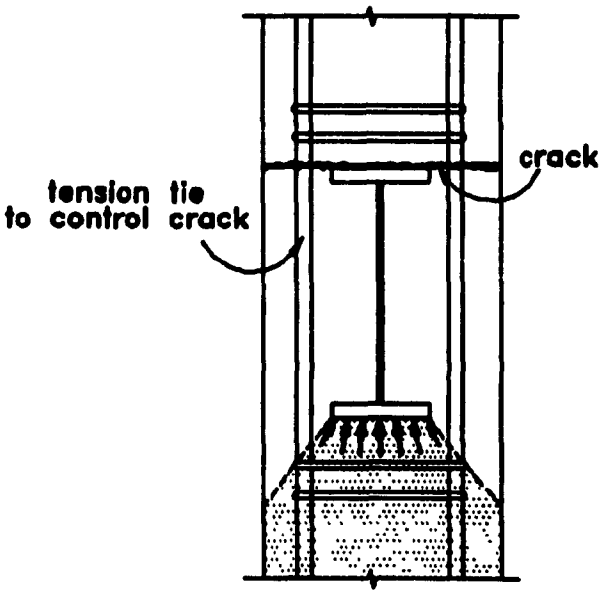

Figure 3.2 Reinforcing steel requirement across the flange-concrete interface

Step 12: Choose the area of vertical reinforcement, such that it is capable of resisting a force equal to the maximum probable shear resistance of the link beam, $1.27V_r$. Thus the area of steel required is:

$$A_s = \frac{1.27V_r}{f_y} \qquad (3.8)$$

The steel required to develop this force must be arranged over the embedment length of the link beam.

The steel requirement calculated in this step is a minimum area requirement and need not be in addition to the concentrated flexural reinforcement of the wall. It is important, however, to ensure that the gap controlling steel is located close to the face of the wall. In this case it will

be most economical to limit the region of concentrated reinforcement to a length no greater than that of the embedment.

The link beams were designed for the prototype structure, given in Chapter 2, using an applied factored shear, V_f, equal to 260 kN. In applying the procedures described above for the design of the test specimen, the material resistance factors, ϕ, ϕ_c and ϕ_s, were taken as 1.0. The complete design and detailing of the link beam, Specimen 1, using specified material properties, are given in Appendix A.

3.1.3 Description of Specimen 1

Figure 3.3(a) shows the details of the link beam design for specimen 1. The link beam has a clear span of 1200 mm and an embedment length, at each end, of 600 mm, bringing the total length of the beam to 2400 mm. The beam was designed as a built-up section with a 3/4 inch (19.2 mm) flange and a 3/16 inch (5 mm) web. The overall height of the section was 350 mm. The section was designed following the procedure described in Section 3.1.1, so that the ultimate shear capacity could be developed while the section remained elastic in flexure. Full-depth, 10 mm thick stiffeners having a spacing of 120 mm, were provided on one side of the web along the clear span. As well as inhibiting web buckling, these stiffeners delay flange buckling. Stiffeners on both sides of the web were provided at each end of the clear span. No stiffeners were located along the embedment lengths. The design of Specimen 1, using the measured material properties and dimensions, is given in Appendix A.

3.1.4 Refinements to the Design Procedure for Specimen 2

The link beam of Specimen 1 underwent significant inelastic deformations along the embedment length, which resulted in significant shear deformations, web crippling and flexural hinging of the link beam along the embedment (see Chapter 5). Refinements were made to the design procedure of Specimen 2 in order to avoid these problems. The shear and local buckling resistances of the link beam web in the embedment were increased in order to ensure that this region remained elastic.

The refinements to the design procedure given above are as follows:

Step 5A: In order to ensure that the link beam remain elastic along its embedment, the embedded region is designed for a factored shear resistance, V_r, of:

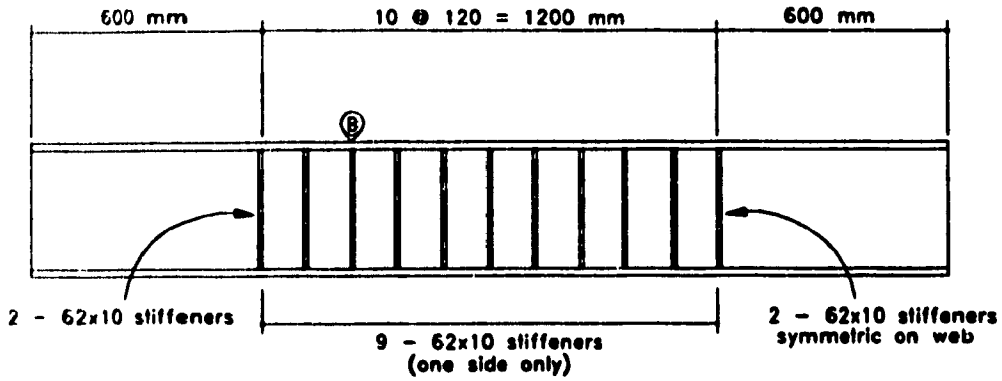

(a) Specimen 1

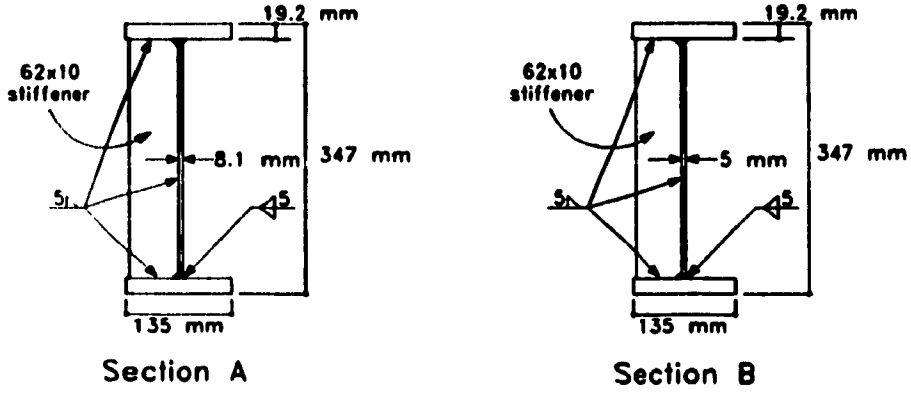

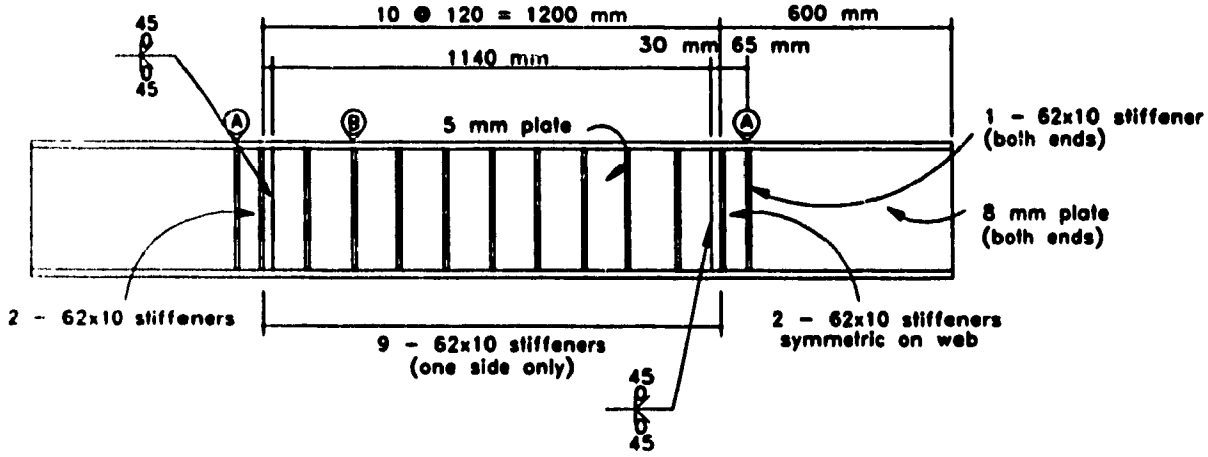

(b) Specimen 2

Figure 3.3 Details of link beam Specimens 1 and 2

$$V_f = \frac{M_f}{\frac{L}{2}} \qquad (3.10)$$

thus, the required web thickness, t_w, for the embedded region can be found using the Equation 3.1 as:

$$t_w = \frac{V_f}{0.55hF_y} \qquad (3.11)$$

Step 7A: Since spalling of the unconfined concrete cover occurs due to reversed cyclic loading, an additional intermediate stiffener is provided at a distance equal to the concrete cover from the face of the wall. This additional stiffener, located where the compressive strains in the concrete are greatest after spalling, serves to prevent flange buckling and web crippling.

Step 11: To account for cover spalling, the effective length of embedment, L_{eff}, is reduced to the actual embedment length minus the concrete cover, L_e - c (see Fig.3.4). Hence, the lever arm, e, measured to the centre of the effective embedment is

$$e = \frac{L}{2} + \frac{L_{eff}}{2} + c \ .$$

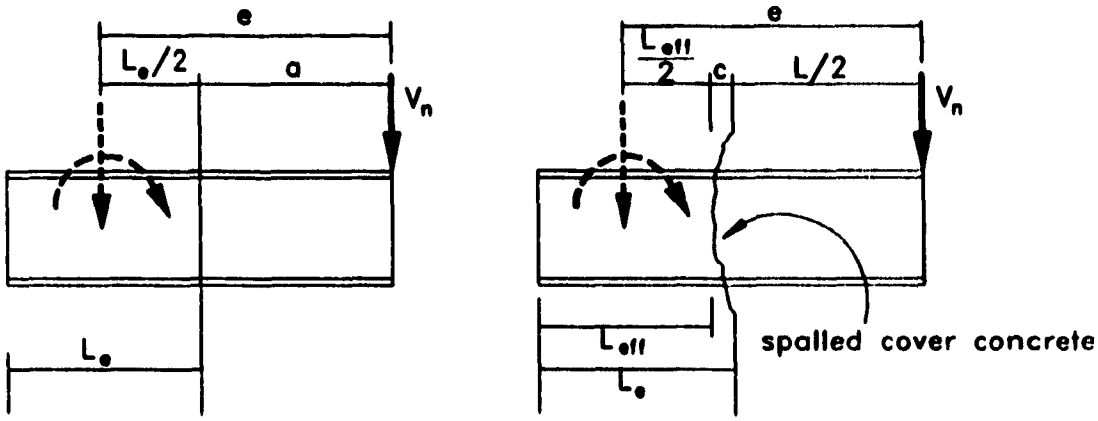

Figure 3.4 Effective length of the embedment

Specimen 2 was designed, including these refinements to the procedure, using the same design shear and material resistance factors as Specimen 1.

3.1.5 Description of Specimen 2

Figure 3.3(b) shows the details of the link beam for Specimen 2. The dimensions of Specimen 2 are identical to those of Specimen 1. The only change in the design of the link beam cross section is that the web of the beam in the joint region was increased to 5/16" (8 mm) thick. This change ensures that the embedded region of the link beam will remain elastic when the shear capacity of the 3/16" (5 mm) thick web in the clear span is developed. The stiffening details in the clear span are identical to those of Specimen 1. An additional stiffener has been added in the joint region of the link beam, at a distance from the face of the wall of 65 mm, corresponding to the location of the first vertical reinforcing bar (see Figure 3.5). This stiffener was added in order to ensure that there is no web crippling in the joint region after the cover concrete has spalled.

3.2 Design of the Walls

The walls for Specimens 1 and 2 are identical and are shown in Fig. 3.5. Each wall has 6 No.25 vertical bars arranged over the embedment length of the link beam. This reinforcement was chosen to provide sufficient tensile capacity over the embedment to equilibrate the compressive resultant in the embedded region. This load was found to be 1176 kN. An additional 2 No.25 bars were located at the back of the wall.

Two No.10 (11.6 mm dia.) horizontal ties were provided at both the top and bottom flange of the link beam to anchor the compressive struts generated by the assumed rigid body rotation of the link beam. The remaining horizontal ties were placed at 260 mm centres, in accordance with the requirements of CAN/CSA A23.3-M89 Clause 21. Additional ties were located at the top and bottom of the walls to provide confinement in the event the walls rotated on their supporting beams.

Two sets of No.10 vertical bars were also supplied at 300 mm centres to conform to Clause 21 requirements.

The vertical bars were welded directly to the support beams in order to ensure the homogeneous movement of the specimen and test frame.

A photograph of the reinforcing cage with the beam in place is shown in Fig. 3.6.

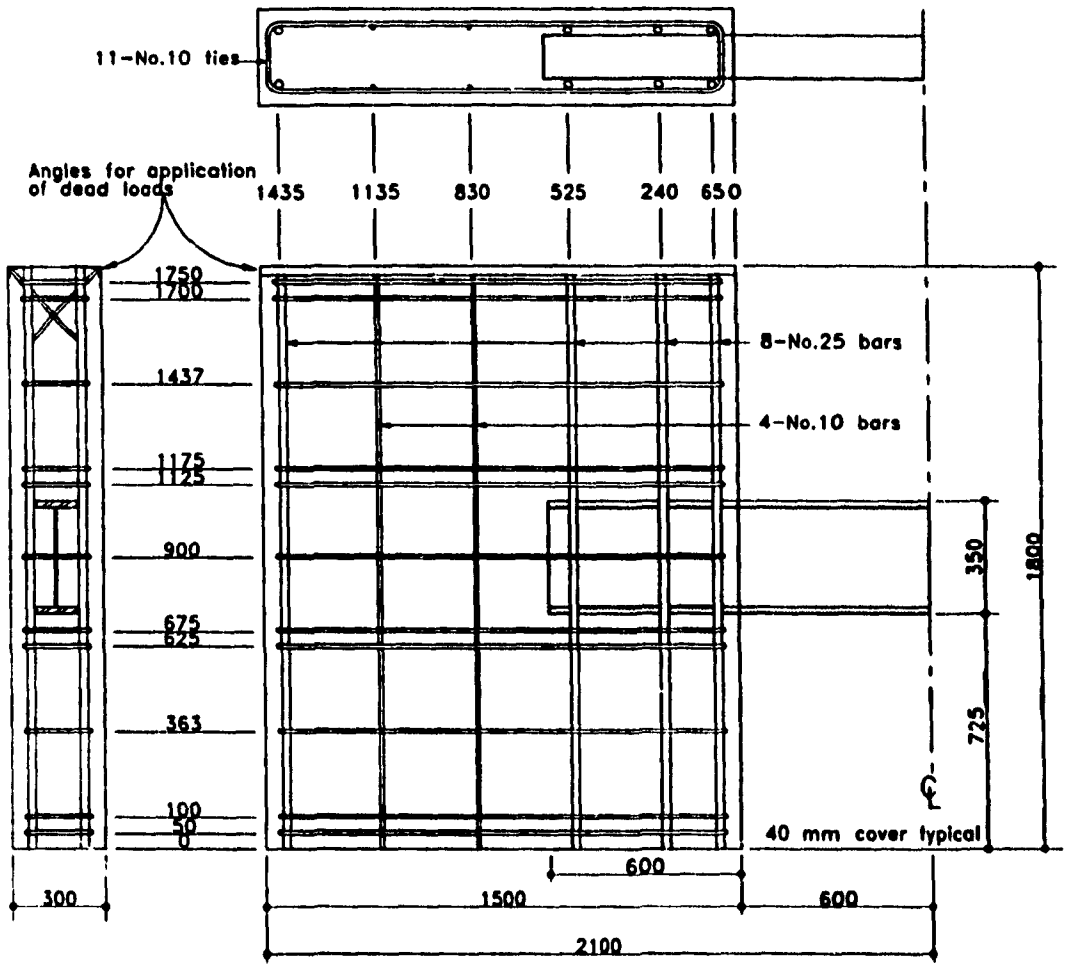

Figure 3.5 Details of reinforcing cage of both specimens

3.3 Material Properties

3.3.1 Reinforcing steel

In accordance with Clause 21.2.5.1 of CSA-A23.3-M84, reinforcing bars conforming to CSA standard G30.16-M were used. Tension tests were performed on 300 mm lengths of each bar size. The applied load and the extension over a 50 mm gauge length were recorded up to the onset of strain hardening. The results of the tension tests are reported in Table 3.1. The reinforcing steel from the same heat was used for both specimens.

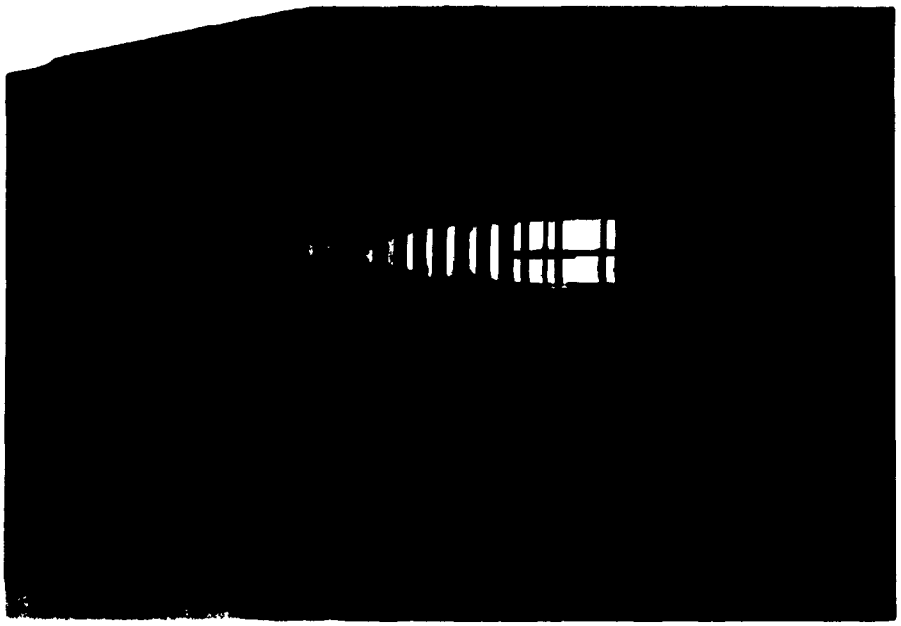

Figure 3.6 reinforcing cage and link beam of Specimen 1

Bar size	Yield stress	Ultimate Stress	Elongation at Rupture
No.10	458 MPa	740 MPa	19
No.25	410 MPa	676 MPa	14

Table 3.1 Properties of reinforcing steel

3.3.2 Concrete

Ready-mix concrete with a minimum specified 28-day compressive strength of 30 MPa and a specified slump of 150 mm, was used in the fabrication of the walls. In order to increase the workability, a plasticising agent, "flowmix", was added to the batches on site.

A number of 150 x 300 mm cylinders and 150 x 150 x 600 mm flexural beams were prepared from each concrete batch. Compression and splitting tests were performed in order to determine the compressive strength, f_c', and the tensile strength of the concrete, f_{sp}, respectively. Testing of Specimen 1 began 38 days after casting and was completed 52 days after casting and testing of Specimen 2 began 37 days after casting and was completed 46 days after casting. The concrete material properties and the age at which they were determined are reported in Table 3.2.

Concrete from Specimen Number	Compressive Strength	Tensile Strength	Modulus of Elasticity
1	25.9 MPa (at 43 days)	1.74 MPa (at 45 days)	24875 MPa
2	43.1 MPa (at 42 days)	3.84 MPa (at 39 days)	30448 MPa

Table 3.2 Properties of concrete

Figure 3.7 illustrates the representative stress-strain relationships determined for the concrete used in each specimen.

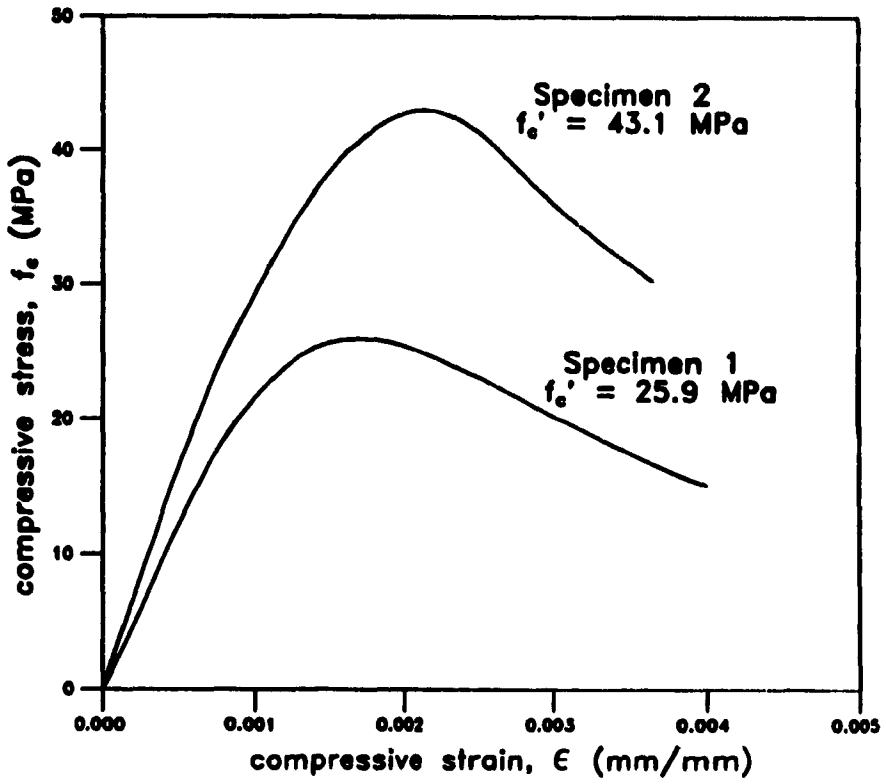

Figure 3.7 Stress-strain relationship for concrete used in Specimens 1 and 2

3.3.3 Link Beam Steel

The link beams were fabricated from Grade 300W material conforming to CSA Standard G40.21 (CSA, 1985). Tension tests were performed on three coupons cut from each sample

provided for the web and flange material. The tension tests were carried out according to the procedure defined in ASTM Standard E8-85a (ASTM, 1985). Applied load and extension over a 50mm gauge length were recorded up to the onset of strain hardening, ultimate load and extensions were also noted. Yield was determined using the offset method with a yield strain of 0.2%. The results of the tension tests are reported in Table 3.3. The 10 mm stock from which the stiffeners were fabricated was not tested. Figure 3.8 illustrates the stress-strain relationships for the steel used in the webs of each specimen.

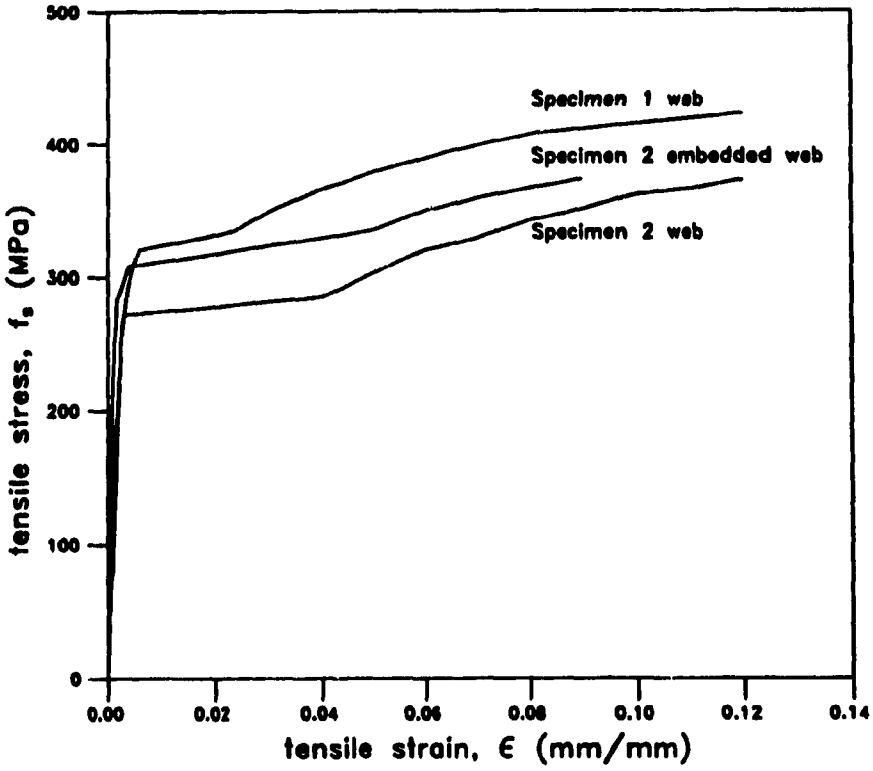

Figure 3.8 Stress-strain relationship for web steels used in Specimens 1 and 2

Steel Specimen	Yield stress	Elongation at onset of strain hardening	Ultimate Stress	Elongation at rupture
Specimen 1 Web	320 MPa	3.2%	468 MPa	32%
Specimen 1 Flange	372 MPa	4.4%	544 MPa	36%
Specimen 2 Beam Web	309 MPa	4.0%	427 MPa	37%
Specimen 2 Embedded Web	276 MPa	4.0%	442 MPa	34%
Specimen 2 Flange	295 MPa	2.4%	499 MPa	39%

Table 3.3 Properties of link beam steel

Chapter 4
Experimental Procedure

4.1 Test Set-up

The overall test set-up is shown in Figure 4.1. The loads and reactions were applied to the walls with two loading beams at the base of each wall. The longitudinal reinforcing bars of both walls were welded to the loading beams. The west loading beam was post-tensioned to the reaction floor of the laboratory with threaded rods. The resulting force clamping the west wall to the floor was 800 kN (670 kN on the east and 130 kN on the west rods), or about twice the expected ultimate applied load. During testing the west wall is expected to remain fixed to the reaction floor.

Figure 4.2 illustrates the manner in which the test set-up simulates the relative displacement, δ, between the two walls which remain essentially parallel

The east wall is loaded vertically such that it remains parallel to the west wall. The reversed cyclic loading applied to the east wall simulates the effects of seismic loading. Loads are applied to the loading beam of the east wall by two loading systems, one passing through the midspan of the link beam and the other at the east end of the wall. During testing these loads are applied such that the east loading beam remains horizontal. In order to produce reversed cyclic loading, two separate jacking systems were provided. For upwards loading, a single 120 kip (530 kN) hydraulic ram reacted against the bottom of the east loading beam directly under the midspan of the link beam. For downwards loading, two 60 kip (267 kN) hydraulic rams under the reaction floor produced tension in the threaded rods attached to the loading beam. To maintain the loading beam in a horizontal position, 60 kip (267 kN) hydraulic rams, located at the east end of the loading beam provided the required levelling forces.

Both walls were restrained from out-of-plane or lateral movement. The top of the west wall was braced with heavy steel angles to a stiff frame. The East wall was restrained against lateral movement with heavy duty rollers fixed to stiff braces.

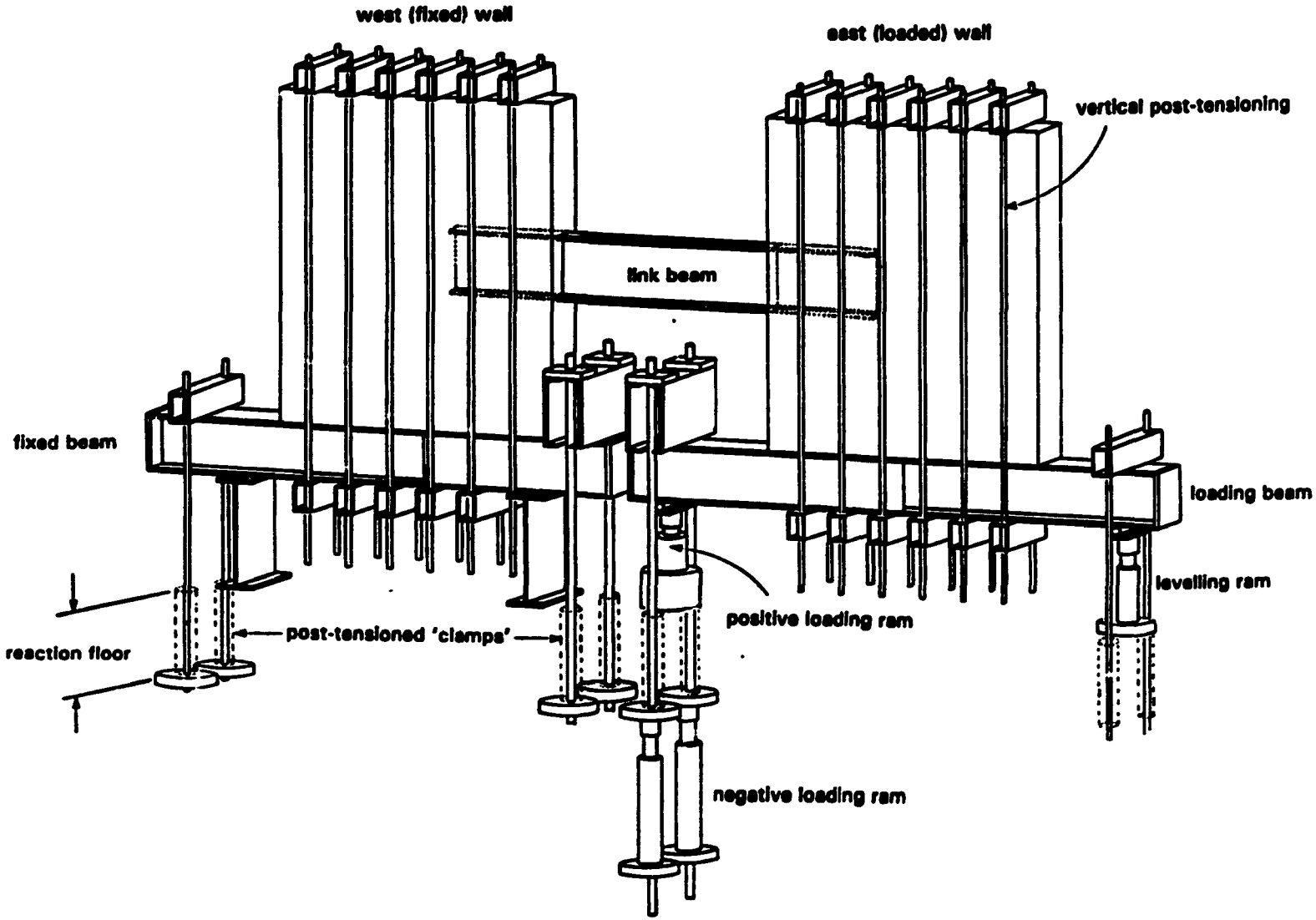

Figure 4.1 Test set-up

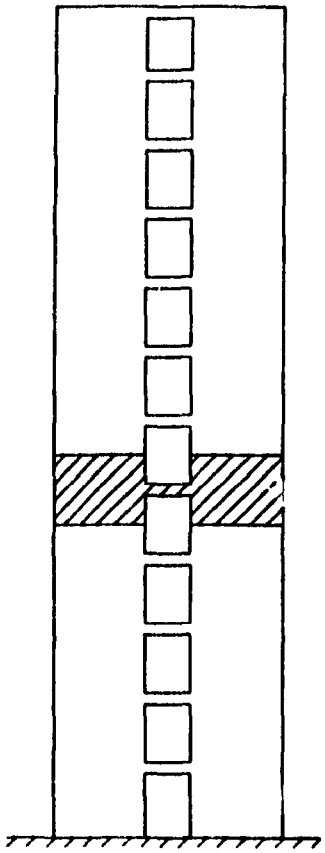

Coupled Wall System

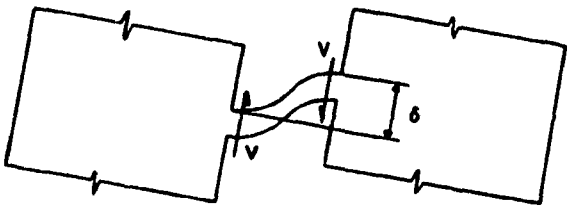

Wall segment in actual structure

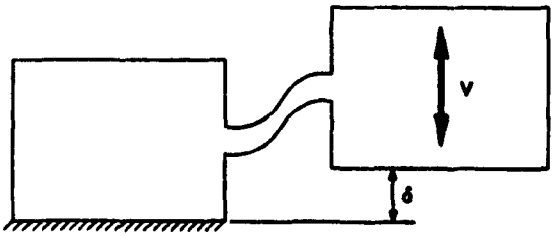

Method of testing wall segment

Figure 4.2 Method of simulating actual coupled wall response

In order to simulate the compressive stresses in the walls due to gravity loads, post-tensioned vertical rods were strapped to the exterior of each wall as shown in Fig. 4.1. Four by six inch (101.6 x 152.4 mm) hollow sections were clamped around the top of the wall and the bottom of the loading beam with one inch (25.4 mm) high strength threaded rods. Each rod was post-tensioned with 25 kips (111 kN). The rods were spaced at 9 inch (228.6 mm) centres resulting in a uniform applied pressure of 430 psi (62 kPa) on each wall.

4.2 Instrumentation

Figure 4.3 shows the instrumentation used for both specimens. An array of linear voltage differential transformers (LVDTs) measured the vertical displacements of both the concrete walls and the loading beams. This instrumentation allowed the differential movement and the rotations of each wall to be determined. The LVDTs were set up so that they could measure relative displacements of ±150 mm. The predicted ultimate displacement was approximately ±125 mm. Dial gauges attached to the loading beams permitted visual control during loading (see Fig. 4.3(a)).

Ten electrical resistance strain gauges were glued to the reinforcing bars in each wall, six measuring the strains in the main vertical reinforcement at the level of the link beam flanges and four on the horizontal ties located above and below the link beam flanges (see Fig. 4.3(a)).

Five strain gauges were glued to the top and bottom flanges of the link beam to determine the flexural strains in the flanges. In addition, strains were obtained from mechanical strain targets having a gauge length of 200 mm. These targets were punched directly into the surface of the steel. Additional electrical resistance strain gauges were located at the ends of each flange near the flange tips. Strain variation either across the flanges or through the flange width would indicate local flange instability. Three strain gauge rosettes were located along the exposed web of the link beam (on the side without the stiffeners) in order to record the shear strains in the web. Additional strain measurements were taken between mechanical strain targets, punched into the steel at 100 mm gauge lengths. For Specimen 2, two additional strain gauge rosettes were located on the embedded portion of the link beam web, 300 mm into the concrete wall. These strain measurements enabled the determination of shear strains in the embedded link beam web.

For Specimen 2, a total of 12 strain gauges were located on the front faces of the walls, three above and three below the link beam on each wall. These gauges measured the strain distribution across the faces of the walls resulting from the bearing of the link beam flanges.

LVDTs and dial gauges were used to record the differential horizontal displacements of the walls.

As shown in Fig. 4.3(b), Specimen 1 is instrumented with mechanical strain targets over a gauge length of 200 mm in order to determine the vertical concrete surface strains over the embedment region at the face of the wall. Due to in-plane splitting, the cover concrete separated from the embedded regions and hence the strains measured at the concrete surface were not representative of the strains near the embedded region. Therefore these strain targets were not

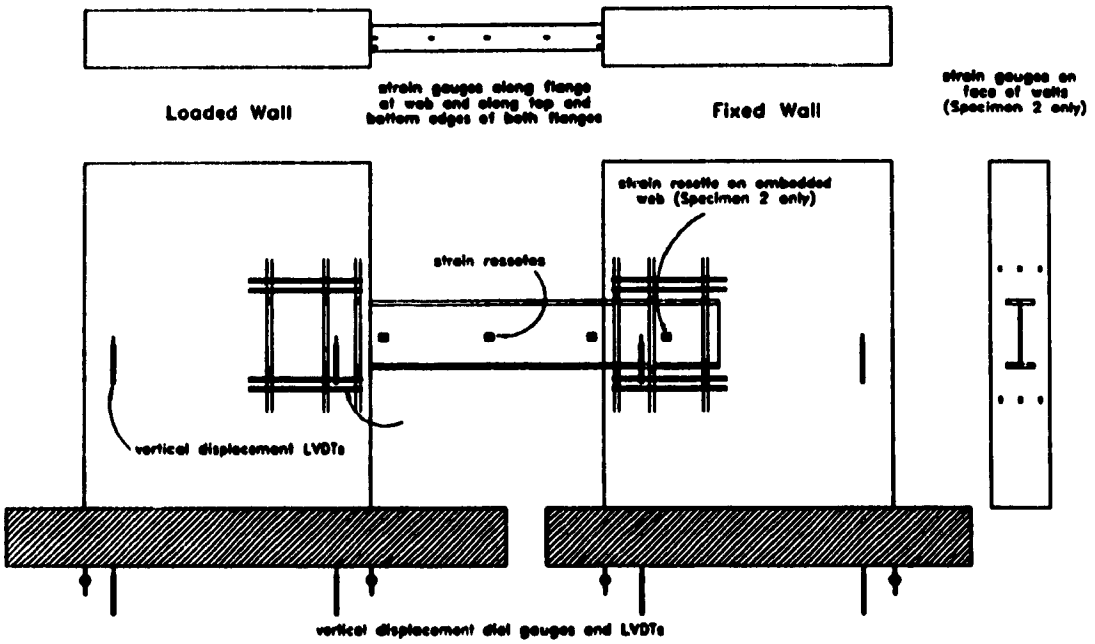

(a) electrical resistance strain gauges and LVDT's

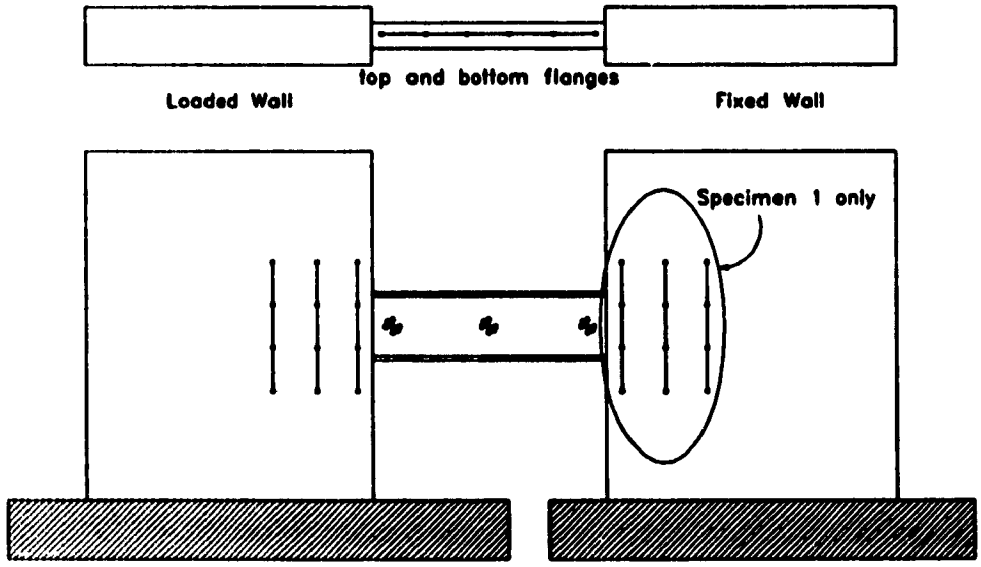

(b) mechanical strain targets

Figure 4.3 Specimen instrumentation

used on Specimen 2.

Loads in the upwards direction were recorded by a 100 kip (445 kN) load cell while loads in the downwards direction were obtained from two 75 kip (334 kN) load cells which recorded the forces in the threaded rods. A load cell was located at the back of the loaded wall in order to record the force necessary to keep the two walls parallel.

The readings from the LVDTs, electrical resistance gauges and load cells were recorded by a Doric 245 data acquisition system and were simultaneously displayed on the screen of an IBM PC.

4.3 Loading History

The loading history for each specimen is shown in Fig. 4.4. In order to control the testing, load versus deflection responses for the east wall were plotted as the testing progressed. Upwards loading and deflections were considered to be positive. In the first cycle, loading was applied to a predetermined peak load followed by three reversed cycles at this load level. This loading control was used until general yielding was observed in the link beam. General yielding was determined when a significant change in the load deflection response was observed, corresponding to observed 'flaking' of the whitewash on the link beam web. After general yielding the peak loading of subsequent cycles was controlled by deflection, with peak deflections taken as multiples of the deflection at general yielding, δ_y.

4.3.1 Load History of Specimen 1

The first two peak loads (±100 and ±200 kN) represented one third and two thirds of the predicted yield strength, respectively. The third peak load (±250 kN) corresponded to the first sign of yielding along the centreline of the link beam web. The first three peak loads exhibited full elastic behaviour. The fourth peak load (±300 kN) corresponded to general yielding of the link beam web at a deflection of $\delta_y = \pm 12$ mm. Subsequent peak deflections corresponded to $\pm 2\delta_y$, $\pm 4\delta_y$, $\pm 6\delta_y$ and $\pm 8\delta_y$. After the specimen had been cycled three times at a displacement of $\pm 8\delta_y$, it was loaded, monotonically to a displacement equivalent to $+10.5\delta_y$.

4.3.2 Load History of Specimen 2

The first two peak loads (±100 and ±200 kN) represented approximately one and two thirds of the predicted yield strength, respectively. The third load stage (±275 kN) corresponded to general yielding of the link beam web at a deflection of $\delta_y = \pm 11$ mm. Subsequent peak

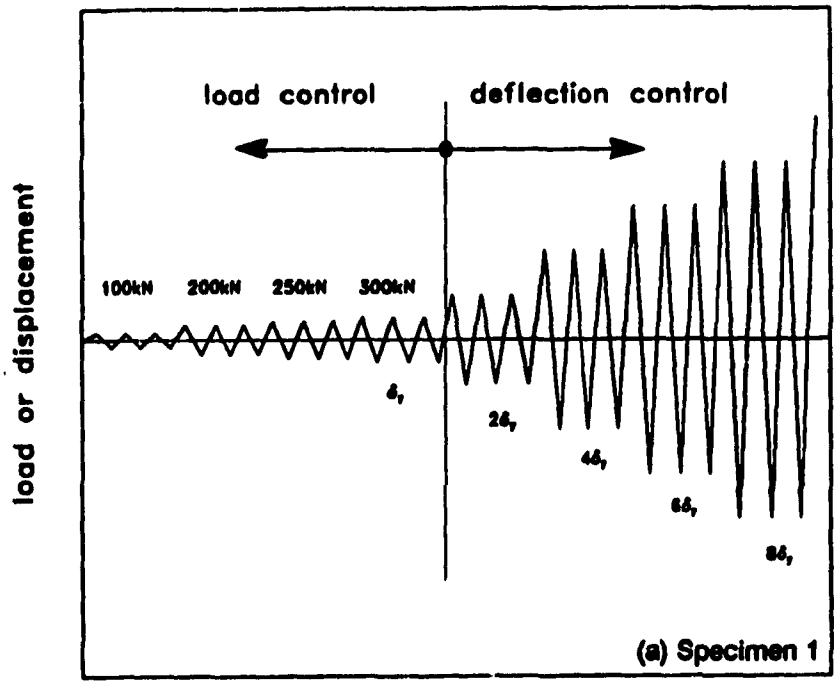

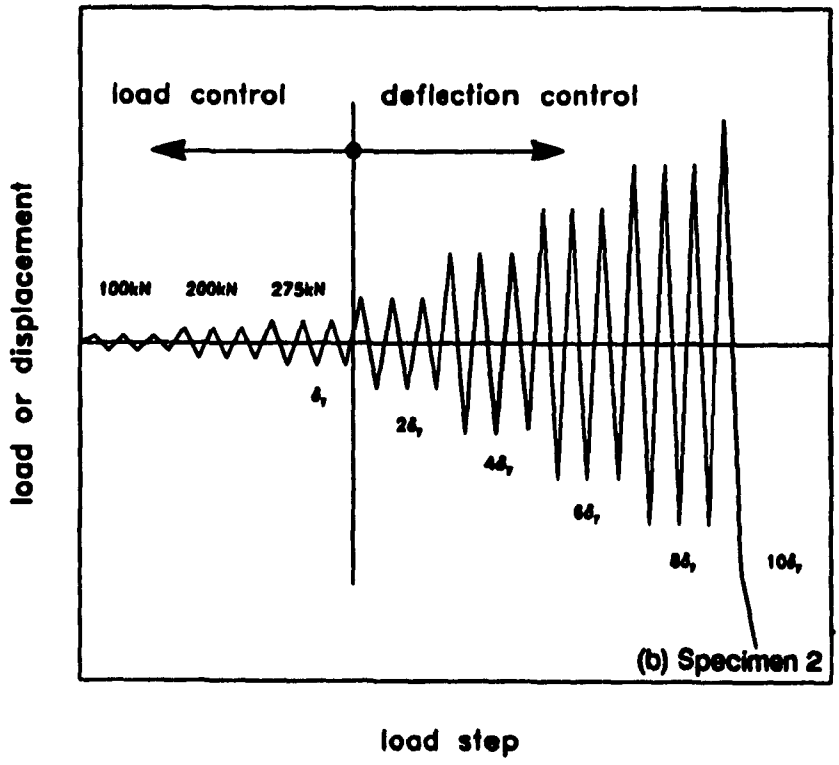

Figure 4.4 Load histories of Specimens 1 and 2

deflections corresponded to $\pm 2\delta_y$, $\pm 4\delta_y$, $\pm 6\delta_y$, $\pm 8\delta_y$ and $\pm 10\delta_y$. After the specimen had been cycled once at a displacement of $\pm 10\delta_y$, it was loaded monotonically to a displacement equivalent to $-13.6\delta_y$.

Chapter 5
Experimental Results

This chapter presents a detailed description of the observed experimental behaviour of Specimens 1 and 2. The letters A and B represent positive (upwards loads and deflections) and negative (downwards loads and deflections) cycles, respectively.

For the load-deflection responses, the load corresponds to the shear transmitted through the link beam and the deflection represents the vertical displacement of the east wall relative to the west wall. The displacements have been corrected to account for measured, differential rotations of the walls. It should be noted that these differential rotations were very small throughout the testing of both specimens and resulted in only minor corrections to the deflections. The key stages in the responses of both specimens are presented in Table 5.1. Detailed observations of each peak load for both specimens are given in Appendix B.

	Specimen 1			Specimen 2		
	Step	Shear (kN)	Defl'n (mm)	Step	Shear (kN)	Defl'n (mm)
first cracking of joint region	4	±200	±4.6	4	±200	±4.9
first local yielding of link beam	7	±250	±6.3	not clearly defined		
general yielding of link beam	10A 10B	303 -300	12.0 -11.1	7A 7B	274 -274	11.2 -9.8
tensile cracking along compressive strut	16B 17A	-385 374	-50.1 50.1	13A 13B	358 -386	44.2 -44.5
ultimate capacity of link beam	19A 19B	388 -409	70.3 -75.5	19B 21A	-446 436	-90.3 88.2
maximum observed deflection	END	344	122.8	END	-361	-150.3

Table 5.1 Summary of critical load stages

5.1 Specimen 1

Figure 5.1 shows the load-deflection response for specimen 1. The first horizontal cracking in the wall, at the level of the link beam flanges occurred at peak loads 4A and 4B corresponding to shears of ±200 kN. From the strain rosette readings, local shear yielding first occurred at the midheight of the link beam web at a shear of ±250 kN, at peaks 7A and 7B. From elastic analysis, based on the measured yield stress of 320 MPa in the web material, the predicted yield shear is 292 kN.

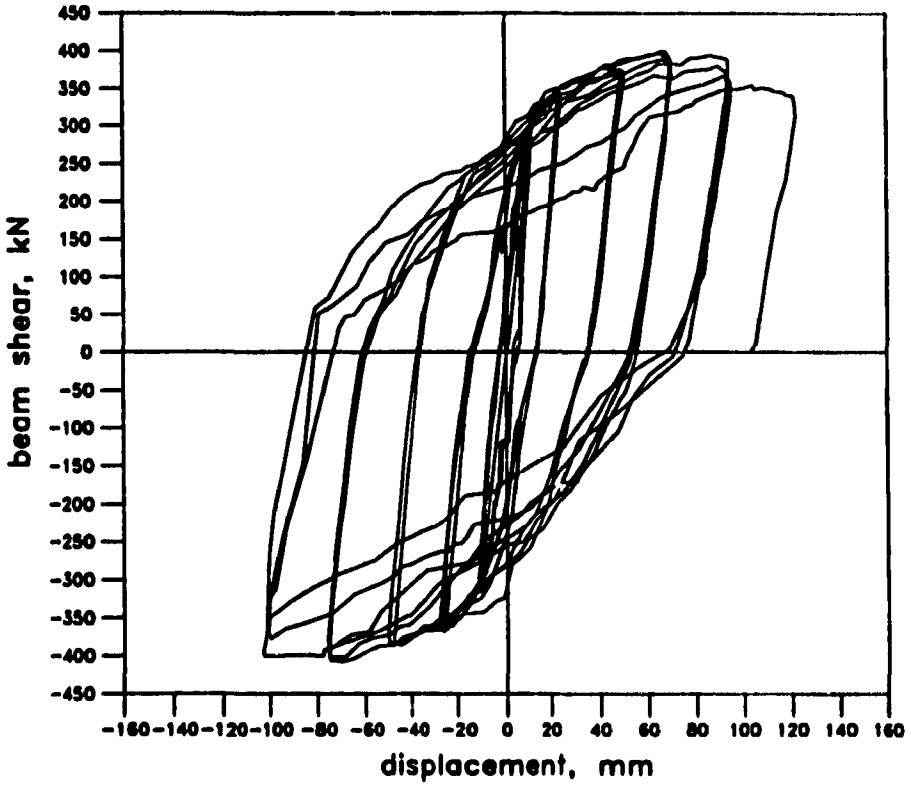

Figure 5.1 Link beam shear versus relative vertical displacement of Specimen 1

General yielding of the link beam web, occurred at peak load 10A, at a load of 303 kN and a vertical displacement of 12.0 mm. At this stage, flaking of the whitewash on the link beam web occurred and there was a noticeable change in the load-deflection response. General yielding in the negative direction occurred at peak load 10B, at a load of -300 kN and a displacement of -11.5 mm. The predicted yielding shear is ±308 kN. The peak displacement, δ_y, at general yielding, was taken as ±12 mm.

Peak shear values were recorded at peak loads 19A and 19B, with values of 388 kN and -409 kN, respectively. The displacements at these peaks were 70.3 mm and -75.5 mm, respectively, corresponding to about $\pm 6\delta_y$. The predicted value for the ultimate shear capacity is 392 kN, assuming that a shear equal to 1.27 times the general yield shear can be attained.

After peak load 19 a reduction in stiffness in the load deflection response was observed with cycling and the peak load values began to decline. By the end of peak loads 24A and 24B, corresponding to displacements of $\pm 8\delta_y$, or ± 96 mm, the peak load values had decreased to 359 kN and -328 kN respectively. The recorded displacements were 95.2 mm and -100.6 mm.

The specimen was finally loaded monotonically in the positive direction to a peak load of 344 kN and a peak displacement of 122.8 mm, that is, about $10\delta_y$. The test was stopped at this stage due to lack of travel of the loading system. It is important to note that in the latter stages of loading that the peak loads attained did not drop below 80% of the maximum capacity obtained. A photograph of Specimen 1 after testing is shown in Figure 5.2.

Figure 5.2 Specimen 1, after testing

5.1.1 Link Beam Response

The link beam performed very much as predicted at both yield and ultimate loads. The predicted values for shear yield and ultimate were 308 kN and 392 kN, respectively. The observed values were 303 kN at yield and 409 kN at ultimate. The predicted ultimate flexural capacity was computed to be 263 kN•m, corresponding to an applied shear force over 438 kN over the 1200 mm clear span. Figure 5.3 shows the measured strains in the flange of the link beam near

the end of the clear span. As can be seen, first yielding was measured in the flange of the link beam at about $4\delta_y$. Two factors contributing to the premature local yielding of the flange where the increase in clear span due to both spalling and outward ratcheting of the link beam, and the distress caused by crippling of both the web and flange in the embedment. Apart from the localised yielding of the flange, very little flexural deformation of the link beam was observed during the test. The large non-recoverable tensile strains exhibited in the later stages of the test (see Fig. 5.3) are a result of the local flange buckling, in the vicinity of the strain gauges, brought about by crippling of the web at the spalled face of the wall. Crippling of the web in the embedment was estimated to have occurred at peak load 17A with noticeable flexural yielding of the last set of stiffeners at the end of the clear span.

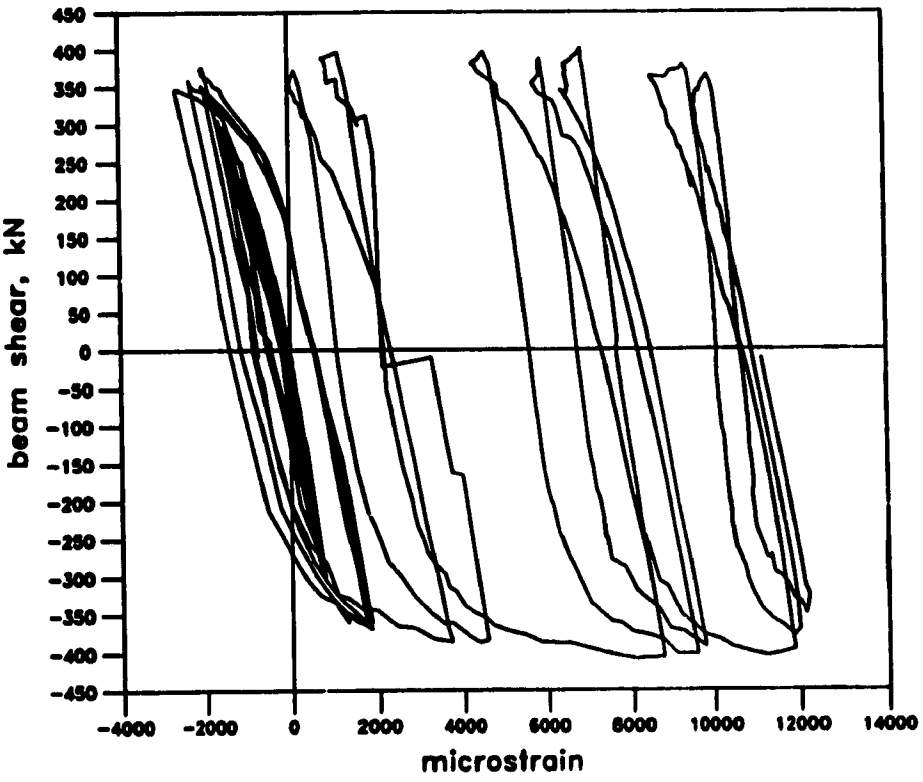

Figure 5.3 Measured strains in the link beam flange of Specimen 1

Figures 5.4 and 5.5 show the link beam embedment just before and after removal from the concrete. The crippling of the web and flange, just inside the embedment, is clearly evident. Tearing of the link beam web occurred at the back of the embedment, in the heat affected zone

of the web-to-flange weld. This tearing, located at the top and bottom of the web, was due to shear yielding of the embedded web.

Figure 5.4 View of east embedment of Specimen 1, with cover concrete removed

Figure 5.4, shows the large gap at the end of the embedment due to the movement of the link beam out of the concrete and the pronounced shear deformation visible at the end of the beam. Significant distress of the link beam web and flanges just inside the embedment and the large gap between the link beam flange and the concrete at the top of the link beam near the front face are also evident. The permanent shear deformation resulted in a relative horizontal movement of 13.2 mm between the top and bottom flanges. The overall height of the section decreased 19.8 mm to 330.2 mm at a location about 75 mm into the embedment. Figure 5.6 shows an overall view of the link beam after removal from the walls.

5.1.2 Reinforced Concrete Response

Stresses in the joint region caused by reversed cyclic loading result in alternating compression zones in the concrete, first at the top and then at the bottom flanges of the link beam near the front faces of the walls. Similar actions occur near the end of the embedment as shown in Fig. 5.7. The first evidence of cracking in the wall was observed at peak loads 4A and 4B, at an applied shear on the link beam of ±200 kN. Horizontal cracks located at the interface between the link beam flanges and the concrete, extended from the flange across the inner face

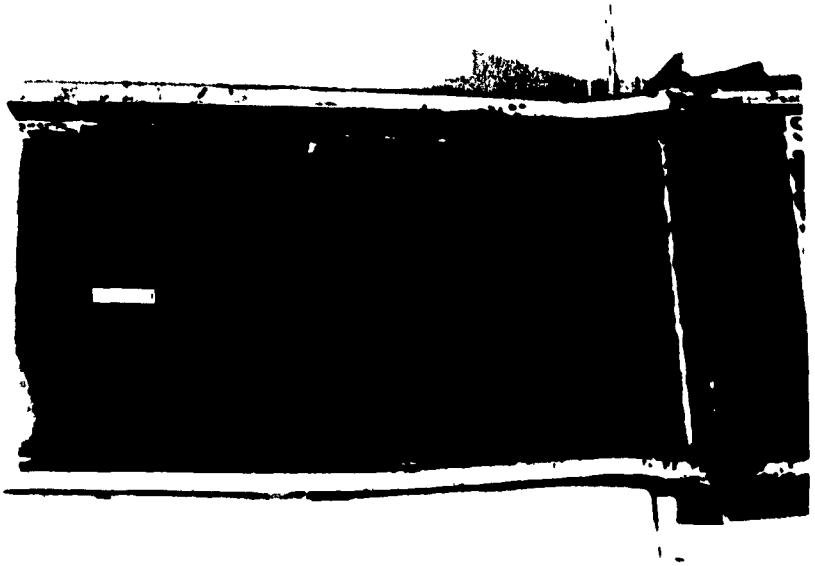

Figure 5.5 View of east end of link beam of Specimen 1 after removal from concrete

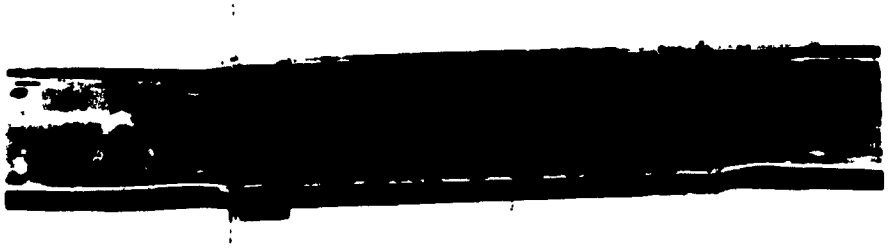

Figure 5.6 Overall view of link beam of Specimen 1 after removal from walls

of the wall to the side faces of the walls (see Fig. 5.8).

Localised spalling and crushing of the concrete along the top and bottom flanges of the link beam, at the front of the compression zone was first observed at peak load 10A, at an applied shear on the link beam of 303 kN. By peak load 13, this distress was evident at all four flange-concrete interfaces. Progressive spalling resulted in a repositioning of the compressive zone further into the embedment region. This phenomenon resulted in an effective increase in the clear span of the link beam (see Fig 5.7b).

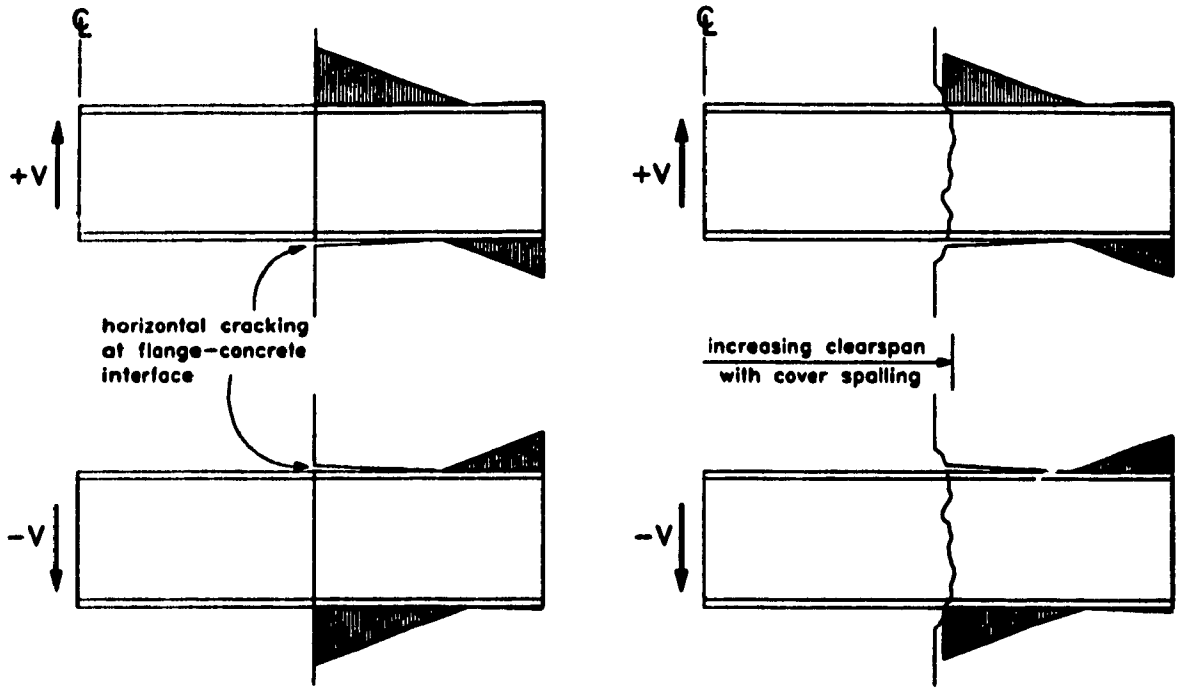

(a) before spalling (b) after spalling

Figure 5.7 Alternating compression zones due to reversed cyclic loading

Further cracking resulted in the spalling of a semi-circular block of cover concrete at the inner face of each wall as shown in Fig. 5.9. At peak load 21A, the outer portions of this detached block of concrete fell off, leaving sound concrete confined between the link beam flanges, which served to stiffen the web in this region. Due to the relative movement between the link beam and the concrete, delamination of the concrete occurred along a vertical plane delineated by the flange tips. Although delamination occurred, the outer concrete is reinforced with the vertical and horizontal reinforcing bars and the concrete between the flanges is confined by the flanges and serves to stiffen the web. The plane of delamination in the east wall at peak load 21A is shown in Figure 5.10.

The first vertical crack appeared in the east wall at peak load 16B, at an applied shear in the link beam of -386 kN. This crack was located 600 mm from the inner face of the wall, the location of the end of the link beam embedment. A similar crack appeared in the west wall,

Figure 5.8 East embedment region of Specimen 1 at peak load 4B

550 mm from the inner face of the wall at peak load 17A.

Vertical and inclined cracks were observed on the east wall at an applied shear in the link beam of -385 kN at peak load 17B. These cracks delineate the direction of principal compressive stresses running from the compressive zones at the flange-concrete interfaces to the loading beam. Such cracking was also evident on the back of the west wall.

A large region of delaminated concrete, determined by a "hollow" sound when tapped, extended about 350 mm above and below the link beam and about 300 mm back into the wall. The crack pattern in this region, as a result of the surfacing of the delamination at peak load 23B is shown in Figure 5.11. Figure 5.11 also clearly shows the cracks indicating the flow of principal compressive stresses.

The severe distress of the embedment region near the inner face of the wall extended about 100 mm into the wall by the final stages of the test, resulting in exposure of the first set of

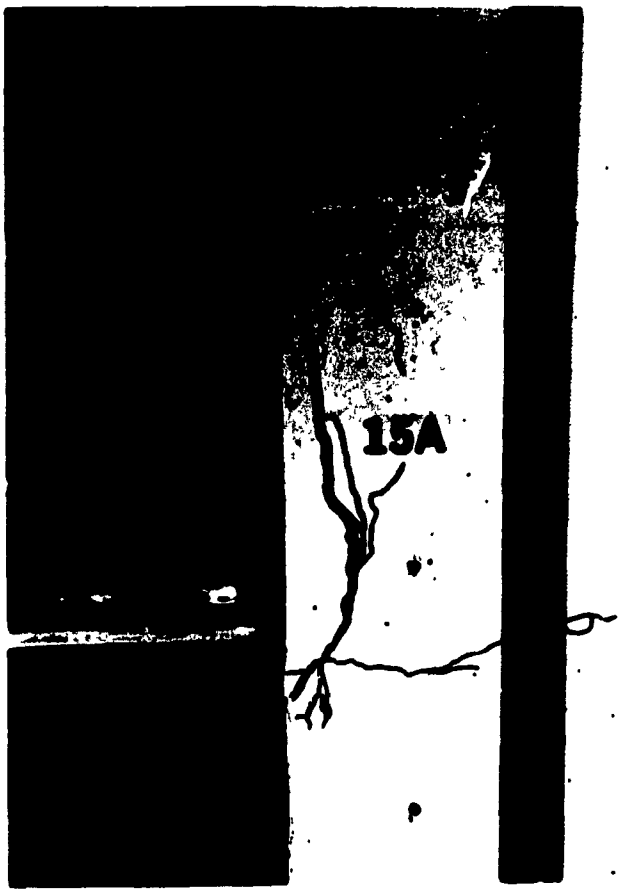

Figure 5.9 East embedment region of Specimen 1 at peak load 15A

reinforcing bars (see Fig. 5.12). The confined concrete immediately above and below the link beam, however, appeared to be sound.

It was not until the final loadstep, when the wall was pushed to a displacement $10\delta_y$ that there was evidence of yielding in the reinforcing bars around the joint region. The horizontal ties above and below the flanges, were clearly just beginning to yield at this final load step.

5.1.3 Hysteretic Response

The response of Specimen 1 (see Fig. 5.1) shows relatively large, stable hysteresis loops up to a ductility level of 6. The hysteresis loops exhibit some 'pinching' as the cracks which form along the top and bottom flanges open and close with the reversed cyclic loading. The loops show very little stiffness degradation until a ductility level of 8 is reached, at which point the stiffness degradation in the loading cycles is very apparent. The peak loads for the displacements at $\pm 8\delta_y$ also show notable decay.

Figure 5.10 Vertical plane of cracking at east embedment region of Specimen 1 at peak load 21A

Figure 5.11 Crack pattern on east wall of Specimen 1 at peak load 23B

Figure 5.12 East embedment region of Specimen 1 at peak load 24B

5.2 Specimen 2

The load-deflection response for Specimen 2 is shown in Figure 5.13. The first horizontal cracking in the wall, at the level of the link beam flanges occurred at peak loads 4A and 4B corresponding to shears of ±200 kN. From strain rosette readings, the first sign of yielding at midheight of the link beam web occurred at a load of about 230 kN, before peak load 7A was reached. From an elastic analysis, based on the measured yield stress of the web material, the predicted shear yield is 262 kN.

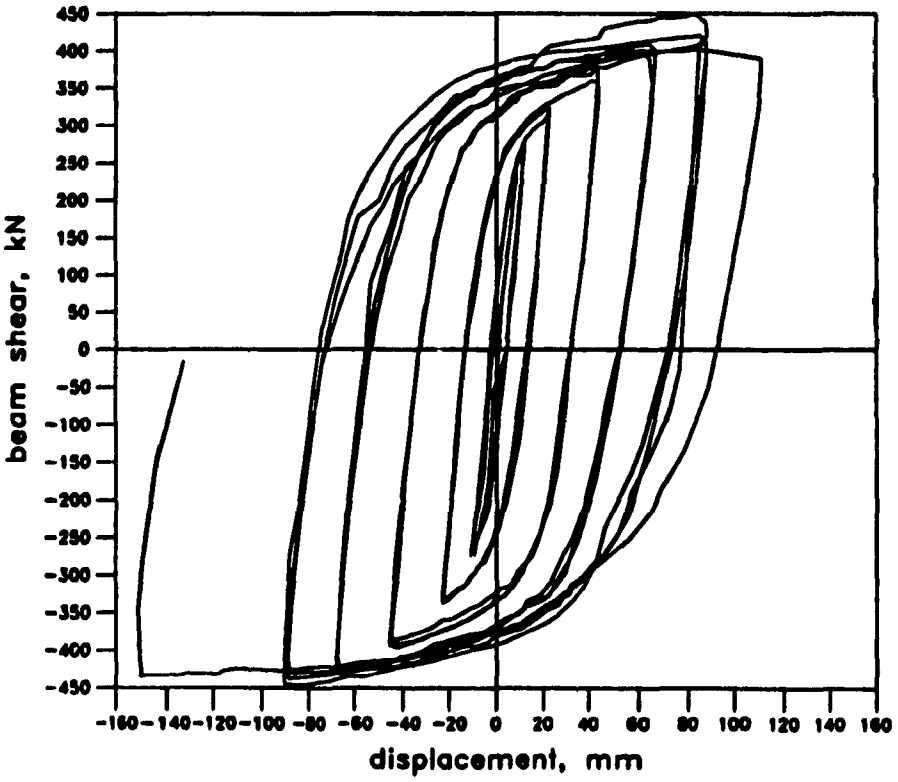

Figure 5.13 Link beam shear versus relative vertical displacement of Specimen 2

General yielding of the link beam web occurred at peak load 7A, at a load of 274 kN and a vertical displacement of 11.2 mm. At this point, the whitewash on the link beam web began to flake and there was a significant drop in the stiffness of the load-deflection response. General yielding in the negative direction occurred at peak load 7B, at a load of -274 kN and a displacement of -9.8 mm. The predicted yielding shear was ±275 kN. The peak displacement, δ_y, at general yielding was taken as ±11 mm.

Maximum shears were recorded at peak loads 19B and 21A, with values of -446 kN and 436 kN, respectively. The displacements at these peak load were -90.3 mm and 88.2 mm, respectively, corresponding to about $\pm 8\delta_y$. The predicted value for the ultimate shear force was 350 kN, indicating that more significant strain hardening was occurring than the 27% stress increase assumed over general yielding.

After peak load 21B some reduction in stiffness in the load-deflection response was observed with cycling and the peak load values began to decline. At the completion of peak loads 22A and 22B, corresponding to displacements of $\pm 10\delta_y$, the peak load values had decreased to 390 kN and -424 kN respectively. The recorded displacements were 110.6 mm and -110.3 mm.

To end the testing, the specimen was loaded monotonically in the negative direction to a peak load of -361 kN and a peak displacement of -150.3 mm, that is, about $13.7\delta_y$ and 15.3 times the actual displacement at general yielding in the negative direction. As with Specimen 1, the peak loads attained after yielding did not drop below 80% of the maximum capacity. A photograph of Specimen 2, after testing, is shown in Fig. 5.14.

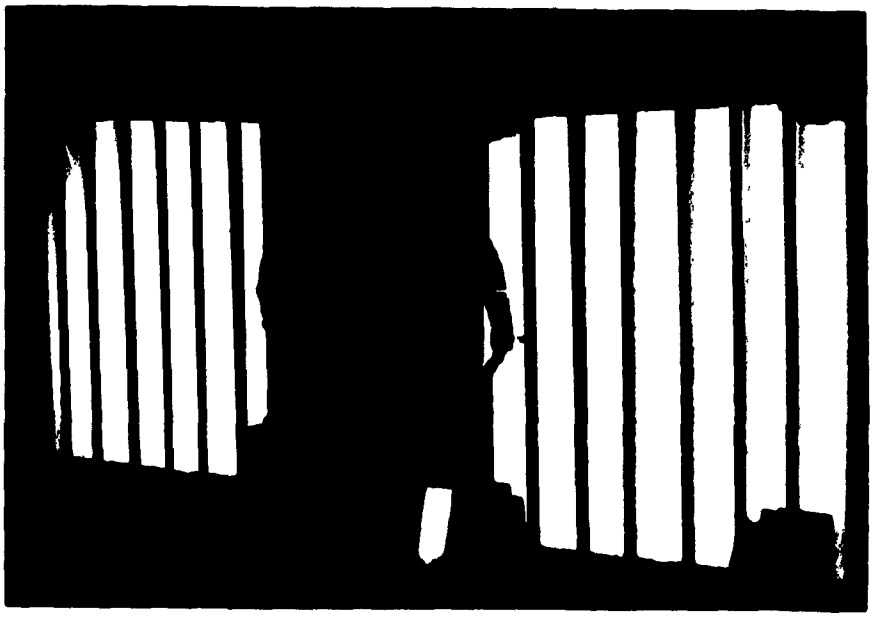

Figure 5.14 Specimen 2, after testing

5.2.1 Link Beam Response

The link beam performed very much as predicted at yield and was found to have considerable reserve capacity before reaching ultimate load. The predicted values for shear yield and ultimate were 275 kN and 350 kN, respectively. The observed values were 274 kN at yield and 440 kN at ultimate. The predicted ultimate flexural capacity was computed to be 249 kN•m,

corresponding to an applied shear force over 415 kN over the 1200 mm clear span. The first signs of flexural yielding of the link beam, in the clear span occurred at peak load 22A, at a deflection of $\pm 10\delta_y$. The flexural capacity of Specimen 2 was not reduced by web crippling at any stage of the test.

The relatively high concrete strength and the thicker link beam web in the embedment resulted in very small rotations of the embedment region. As can be seen in Figs. 5.14 and 5.15 significant shear deformations can be seen over the clear span of the link beam.

Figure 5.15 Overall view of link beam of Specimen 2 at end of testing showing severe web buckling

Web buckling in the clear span was first observed at peak load 18B, and became more pronounced as the test progressed. Fig. 5.15 clearly shows the degree of web buckling by the end of the test. The tension field action, with the associated buckling, between adjacent stiffeners is evident. The shear distress in the link beam was more pronounced by peak load 21B when the web stiffeners showed signs of flexural yielding in double curvature. Once the stiffeners began to yield, some twisting of both flanges was observed, although this did not progress to the point of inducing flange buckling.

The concrete cover at the inner face of both walls had spalled off by peak load 21A, revealing the thicker web in the embedment regions. Although there was little lateral support provided by the concrete for the embedded webs, no evidence of yielding was observed in this region. In the final cycle at $10\delta_y$, strain rosettes on the west embedded web indicated that the web had yielded. Figure 5.16 shows the shear versus shear strain response for the webs of both

embedments. The predicted shear yield for the embedded webs is 419 kN. The corresponding yield strain, from elastic analysis is 1912 $\mu\epsilon$. The east embedment remained elastic throughout the test. Figure 5.17 shows an overall view of the link beam after removal from the walls.

Figure 5.17 Overall view of link beam of Specimen 2 after removal from the walls

5.2.2 Reinforced Concrete Response

The first evidence of cracking in the wall was observed at peak loads 4A and 4B, at an applied shear on the link beam of ±200 kN. Horizontal cracks located at the interface between the link beam flanges and the concrete, extended from the flange across the inner face of the wall to the side faces of the walls (see Fig. 5.18).

Further cracking resulted in the spalling of a semi-circular block of concrete at the inner face of each wall. Figure 5.19 shows the cracking of the east embedment region at peak load 15B. At loadstep 18A, further spalling occurred revealing the well confined concrete of the wall and the sound concrete confined between the link beam flanges. Figure 5.20 shows the delamination between the link beam and the surrounding concrete due to their relative movements.

The first vertical cracks appeared at peak load 8A, at an applied shear in the link beam of 275 kN. The cracks were located 480 and 325 mm from the inner face of the east wall and 730 and 445 mm from the face of the west wall. Vertical and inclined cracks, delineating the direction of principal compressive stresses, were observed on the east wall at an applied shear in the link beam of -337 kN at loadstep 12B. Similar cracks were observed on the west wall at an applied shear in the link beam of 358 kN at peak load 13A. The crack pattern on the east and west walls at peak load 22A are shown in Figs. 5.21 and 5.22, respectively. Both figures clearly show the cracks following the direction of principal compressive stresses from the bottom flange of the embedment to the loading beams. Similar cracking is apparent extending up from the top flange

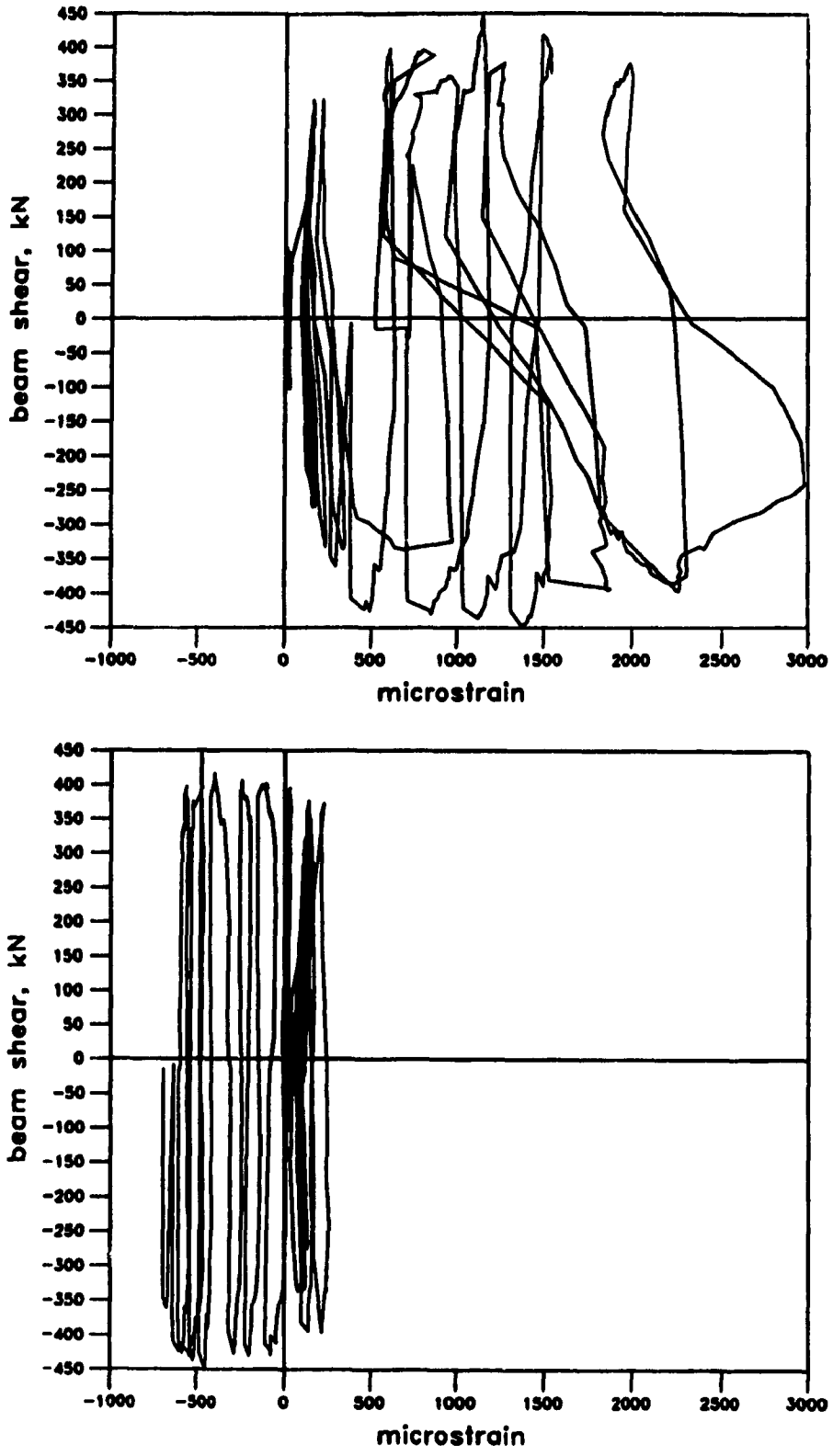

Figure 5.16 Shear versus shear strain response of east (top) and west (bottom) embedded web regions of Specimen 2

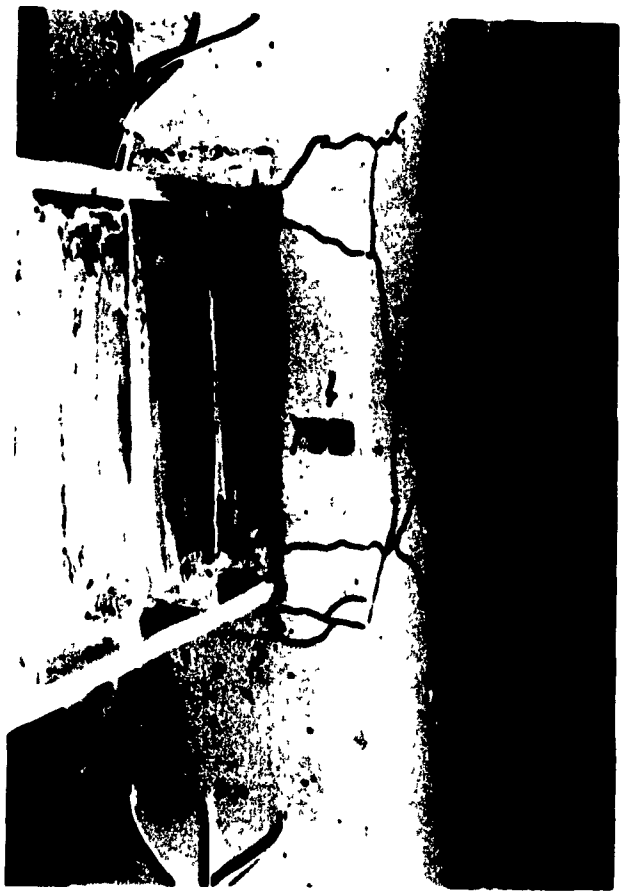

Figure 5.18 East embedment region of Specimen 2 at peak load 98

of the link beam, although due to the more flexible boundary conditions at the top of the specimen, this pattern is less pronounced.

The spalling of the embedment region near the inner face of the wall extended about 100 mm into the wall by the final stages of the test, resulting in exposure of the first set of reinforcing bars (see Fig. 5.23). The confined concrete immediately above and below the link beam, however, appeared to be sound.

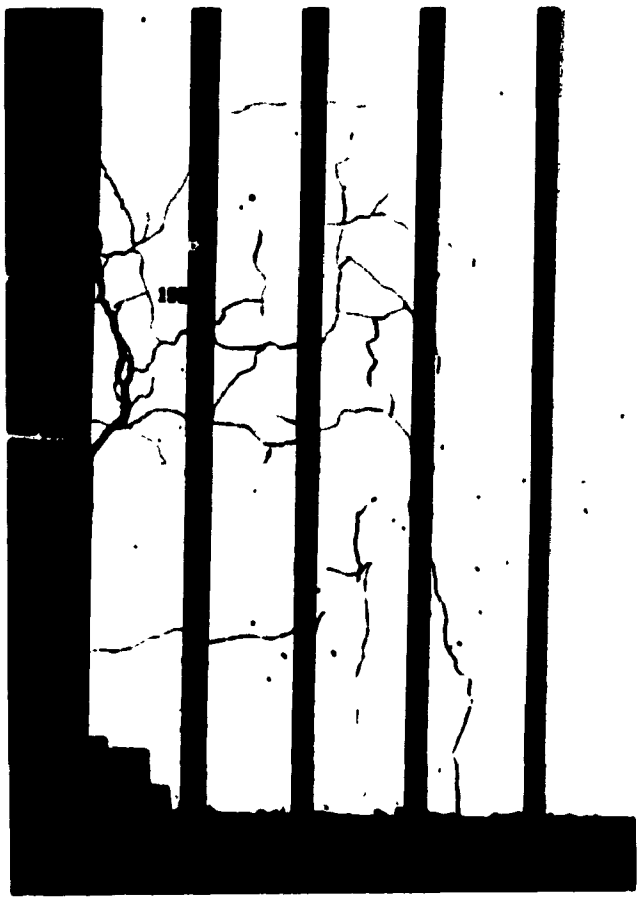

Figure 5.19 East embedment region of Specimen 2 at peak load 15B

5.2.3 Hysteretic Response

The response of Specimen 2 (see Fig. 5.13) shows large, stable hysteresis loops, up to a ductility level of $8\delta_y$. The hysteretic response exhibits behaviour typical of that for steel beams, designed and detailed to yield in shear. Only slight stiffness degradation was noticed when a ductility level of $8\delta_y$ was reached and no strength degradation was observed. The cycle at $\pm 10\delta_y$ exhibited some decay in stiffness and a 20% drop in the peak load value. As the specimen was loaded monotonically at the end of testing to 15.5 times the deflection at yield in the negative direction, very little load and stiffness degradation was evident. The final displacement reached was -150 mm.

Figure 5.20 Vertical plane of cracking at east embedment region of Specimen 2 at peak load 19A

Figure 5.21 Crack pattern on east wall of Specimen 2 at peak load 22A

Figure 5.22 Crack pattern on west wall of Specimen 2 at peak load 22A

Figure 5.23 West embedment region of Specimen 2 at peak load 22A

Chapter 6
Comparison of the Responses of Specimens 1 and 2

6.1 Comparison of Predicted and Experimental Values

Table 6.1 compares the shears corresponding to the key behavioural events for Specimens 1 and 2. The calculations for the predicted values are given in Appendix A. The predicted values for both specimens were calculated using the refined design approach presented in Section 3.1 which accounts for the effect of spalling of the concrete cover. This cover spalling gives rise to an increase in the clear span of the link beam and a decrease in the embedment lengths of the link beam. It is noted that the link beam of Specimen 2 had a lower yield stress and a slightly thinner web in the clear span region. The difference in predicted strengths of the reinforced concrete embedments is due to the significant difference in concrete strengths (25.9 and 43.1 MPa, for Specimens 1 and 2, respectively). The measured cross-sectional dimensions are given in Appendix A. The measured material properties are given in Section 3.3.

As can be seen from Table 6.1, the predicted failure mode of Specimen 1 agrees well with the observed failure mode. This specimen, however, exhibited significant yielding of the embedded web as well as web crippling in the region of cover spalling. Refinements to the design procedure resulted in improved performance of Specimen 2 with full shear yielding occurring in the exposed link beam without significant distress of the link beam in the embedded region. The procedure for the design of the reinforced concrete embedment region was adapted to include the effects of cover spalling and provide reinforcement capable of controlling the flange-concrete interface gap. The responses of both specimens demonstrated that the design of the reinforced concrete embedded region was adequate to develop the necessary capacity and control the gap openings.

	Specimen 1		Specimen 2	
	Predicted	Experimental	Predicted	Experimental
V at first shear yield of link beam (kN)	292	250	262	230
V at general shear yield of link beam (kN)	308	303	275	274
V at first flexural yield of link beam (kN)	412	380	389	did not yield
V at ultimate shear capacity of link beam (kN)	392	409	350	446
V at yield of embedded link beam (kN)	308	≈350	419	yielding only at $10\delta_y$
V at reinforced concrete embedment capacity (kN)	373	was not attained	616	was not attained
Failure modes	shear yielding of link beam	shear yielding of exposed and embedded link beam with web crippling in embedded region	shear yielding of exposed link beam	shear yielding of exposed link beam without distress in embedded region

Table 6.1 Comparisons of predicted and experimental values

6.2 Hysteretic Responses

The complete hysteretic responses of Specimens 1 and 2 are shown in Fig. 6.1. Both responses exhibit excellent energy absorption and stable hysteretic response loops. Specimen 1 begins to show evidence of 'pinching' at a displacement of $\pm 8\delta_y$ in the second and third cycles. The hysteresis loops of Specimen 2 showed excellent repeatability through each cycle at each displacement level with no signs of significant 'pinching'. Only a very minor stiffness decay was observed at displacements corresponding to $\pm 8\delta_y$ and $\pm 10\delta_y$.

The applied shear versus displacement envelopes at ductility levels of $4\delta_y$ and $8\delta_y$ are shown in Figs. 6.2 and 6.3, respectively. The larger loops exhibited by Specimen 2 indicate that a greater amount of energy is being dissipated than in Specimen 1. In assessing the differences between the two specimens, it is important to recognise that the link beam of Specimen 2 had both a marginally thinner web and a smaller yield stress.

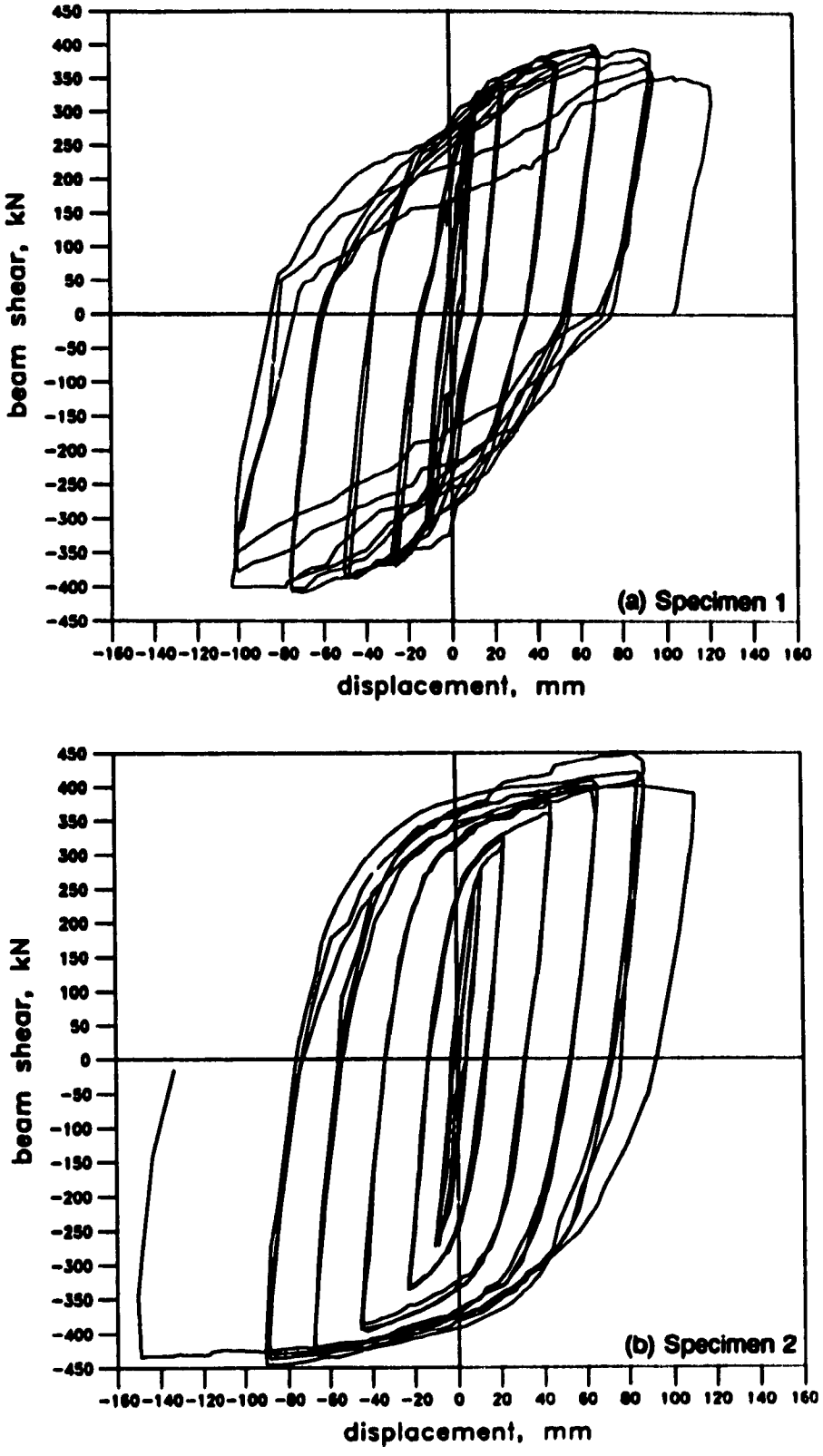

Figure 6.1 Link beam shear versus relative displacement of Specimens 1 and 2

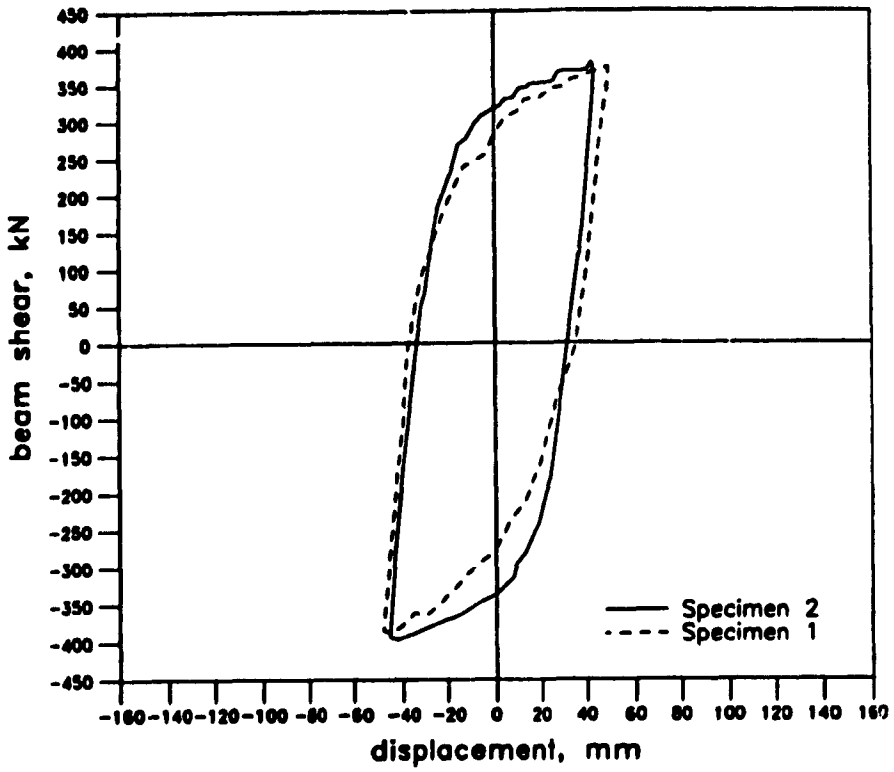

Figure 6.2 Applied shear versus displacement envelope at $4\delta_y$

The cumulative energy curves for both specimens are shown in Fig. 6.4. Due to the distress of the embedded portion of the link beam, the energy absorbing ability of Specimen 1 drops below that of Specimen 2 after a displacement ductility of about 7. This drop in the energy dissipation is due to the 'pinching' evident in the hysteresis loops and the reduction in the load carrying capability (see Fig. 6.1). Specimen 2 continued to exhibit excellent energy absorption capability throughout the entire reversed cyclic loading.

In order to quantify the overall response of each specimen, an equivalent elastic damping coefficient, β, is used. This coefficient, β, is defined as (see Fig. 6.5):

$$\beta = \frac{A_1}{A_2} \times \frac{1}{2\pi}$$

where A_1 is the area within the hysteresis loop of one half cycle, and,
A_2 is the area of the triangle defined by an equivalent elastic stiffness to the peak load and corresponding deflection of each half cycle.

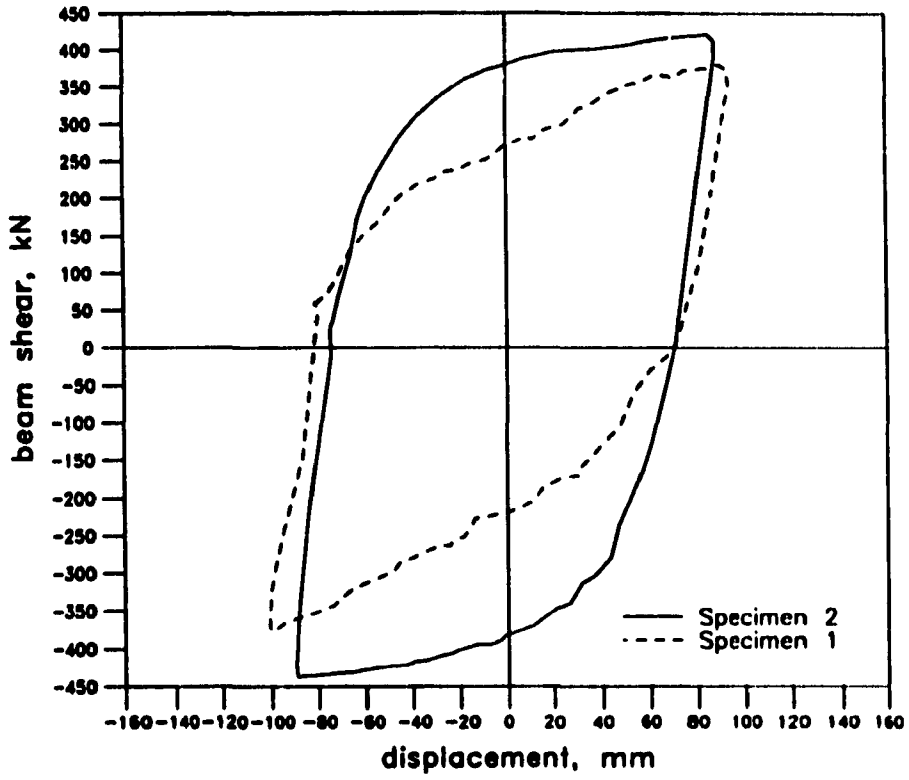

Figure 6.3 Applied shear versus displacement envelope at $8\delta_y$

The maximum value of β, representing the case of rigid-perfectly plastic hysteretic behaviour with rigid unloading response is $\frac{2}{2\pi} = 0.318 = 31.8\%$. The equivalent elastic damping coefficients for each half loop for Specimens 1 and 2 are shown in Fig 6.5.

At each ductility level, the damping coefficient of the first positive half cycle is represented by the top data point while the third negative half cycle is the bottom data point. The width of the response band is an indication of the degree of decay of energy absorption occurring with cycling at each ductility level. A wider band indicates greater decay of energy absorption than a thinner band.

It clear from Fig. 6.5 that Specimen 2 exhibits a higher level of damping, and is therefore able to dissipate greater amounts of energy. It can also be seen that the response of Specimen 1 exhibits significantly greater decay beyond a displacement ductility level of 4.

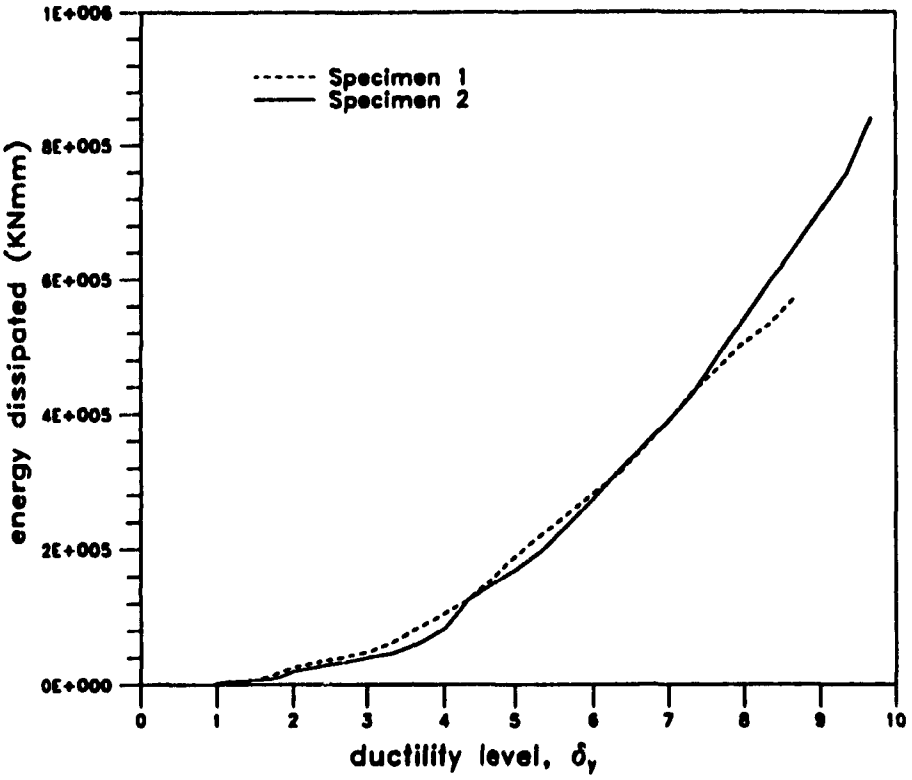

Figure 6.4 Cumulative energy dissipation of Specimens 1 and 2

6.3 Response of the Link Beams

Although Specimen 1 exhibited excellent response characteristics up to a displacement ductility of about 6, severe web crippling occurring in the embedded region (see Section 5.1.1), reduced both the shear and moment capacity of the link beam at the spalled face of the wall. The refinements to the design for Specimen 2 (see Section 3.1.4.) were an attempt to control this failure mechanism.

It was clear that the embedded regions of Specimen 2 behaved as desired, with the steel embedment remaining elastic while the link beam experienced significant deformations over its clear span. Since the crippling of the embedded link beam had been controlled, the embedment region experienced very little distress and the behaviour approaches that of a ductile link beam in an eccentrically braced frame (Engelhardt and Popov, 1989). These design and detailing refinements resulted in virtually rectangular, hysteresis loops which remained stable up to very high ductilities and excellent energy absorption. When web crippling is controlled, there are two

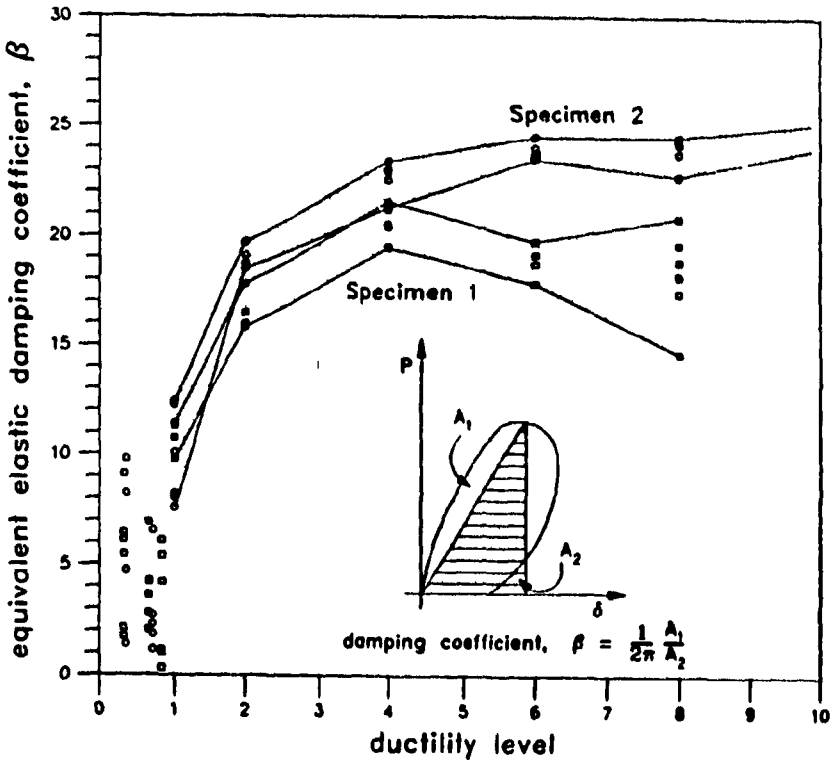

Figure 6.5 Equivalent elastic damping coefficients for Specimens 1 and 2

potential controlling modes of failure; either the web of the link beam will tear as a result of low cycle fatigue or the link beam will buckle laterally. There was no evidence of either of these failure modes in Specimen 2. Figure 6.6 shows the link beams of Specimen 1 (top) and 2 (bottom) after removal from the walls. The crippling of the embedment region of Specimen 1 is very apparent. It can be seen that the only distress to the link beam of Specimen 2 occurred in the clear span.

6.4 Response of the Reinforced Concrete Embedment Regions

The strains in the longitudinal reinforcing steel near the face of the walls in the reinforced concrete embedment regions of Specimens 1 and 2, are illustrated in Fig. 6.7. Before loading, the vertical reinforcement of both specimens exhibited a small compressive strain due to the post-tensioning of the walls to simulate gravity loading. It can be seen that this longitudinal steel does not yield (yield strain = 2000 microstrain) in either wall, indicating that the steel provided served

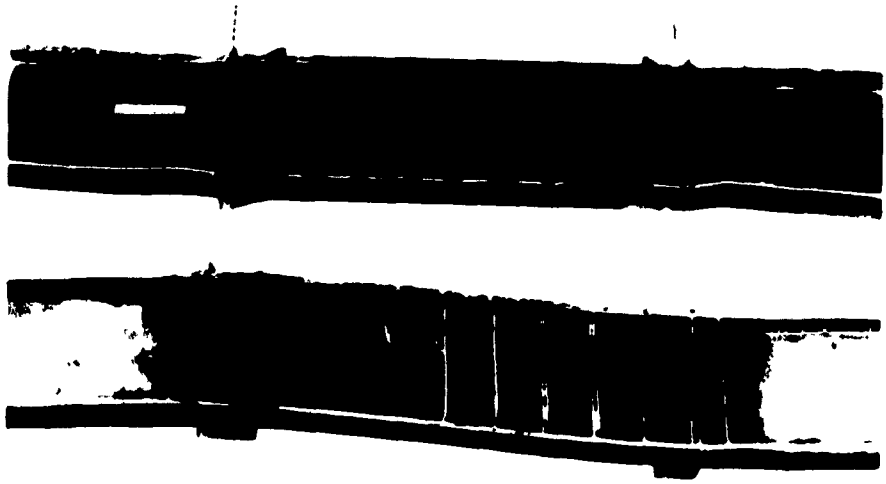

Figure 6.6 Link beams of Specimen 1 (top) and 2 (bottom) after removal from the walls

its function in controlling the horizontal cracking along the flange-concrete interface. With cycling beyond a displacement ductility of about 4, the longitudinal steel strains exhibit non-recoverable tensile strains which increase with each successive cycle. This phenomenon was not significant in Specimen 2 (see Fig. 6.7(b)). Throughout its entire response, the horizontal crack at the flange-concrete interface of Specimen 2, opened and completely closed with cycling. On the other hand, the embedded portion of the link beam of Specimen 1 experienced web crippling in the region of the longitudinal reinforcement. Because of this web crippling the embedded link beam lost a considerable amount of stiffness and, hence, was unable to provide sufficient bearing stresses to completely close the crack.

6.5 Displacement Contributions of the Embedment Regions

It is clear from the hysteretic response of the system and from the relative lack of distress to the reinforced concrete embedment, that the behaviour of the coupled system is dominated by the response of the link beam. Figure 6.8 shows the contribution of the displacements of the link beam to the total relative displacements of the walls for Specimens 1 and 2. The dashed line on each figure represents the relative displacements of the ends of the link beams while the solid line represents the total relative displacements of the walls. For Specimen 1 up to a displacement

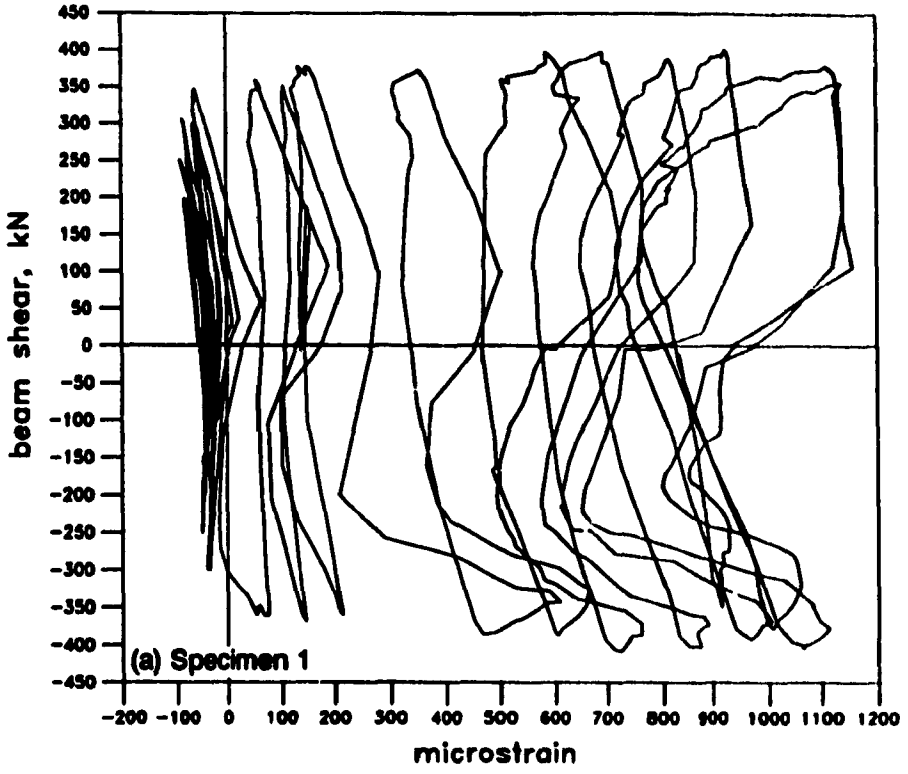

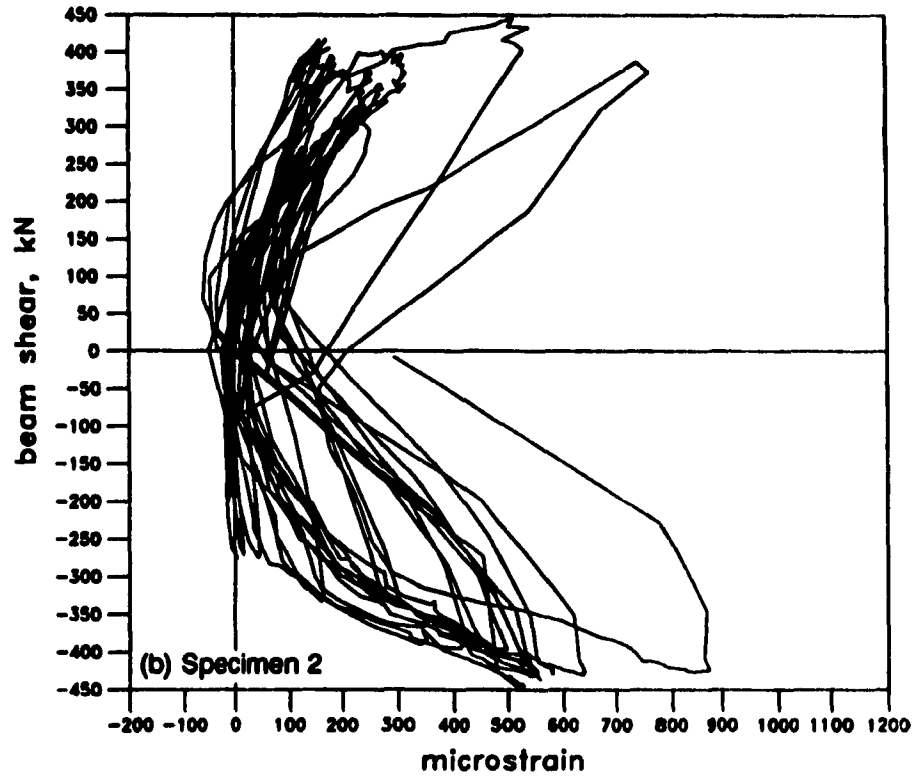

Figure 6.7 Strains in the longitudinal reinforcing bars at the inside face of the east wall

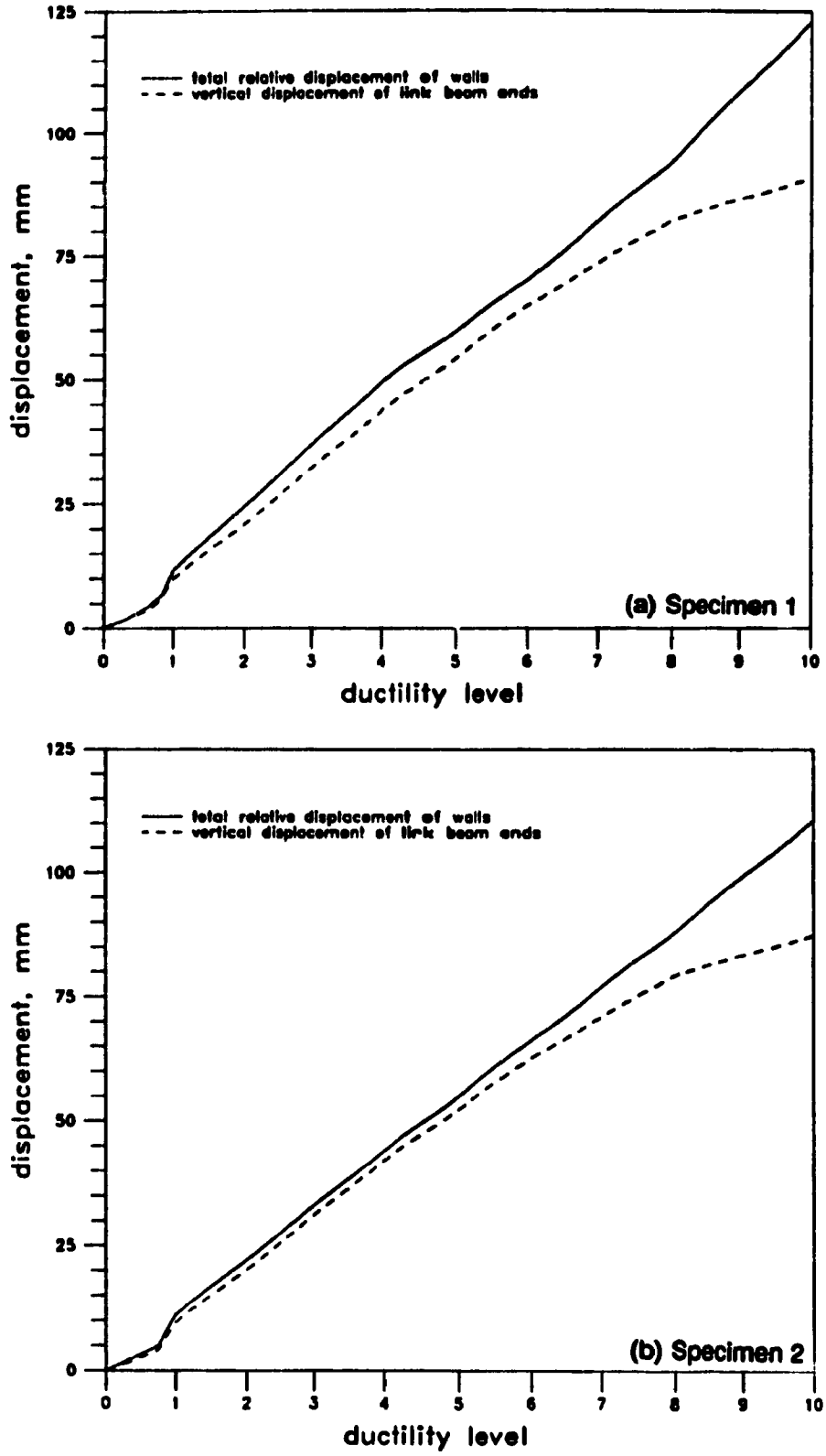

Figure 6.8 Contribution of the displacements of the link beams to the total relative displacements of the Specimens

of $8\delta_y$, the link beam contributes about 92% of the total displacement. The remaining 8% is a result mainly of the inelastic deformations in the embedment. The improved embedment detailing of Specimen 2 reduces this contribution to about 3% of the total displacement.

The increased displacement contribution due to the inelastic response of the embedment and embedded region above a ductility level of about $8\delta_y$ is apparent for both specimens (see Fig. 6.8). It should be noted, however, that even at ductility levels of $10\delta_y$, the link beam continues to represent more than 80% of the total displacement response.

Chapter 7
Assessment of Performance of Steel Link Beams Coupling Reinforced Concrete Walls

In order to assess the performance of steel link beams coupling reinforced concrete walls, the responses of Specimens 1 and 2 will be compared to the responses of common types of coupling beams tested by others.

7.1 Comparisons with Reinforced Concrete Coupling Beams

A discussion of both traditionally reinforced and diagonally reinforced concrete coupling beams is given in Section 1.3. For ductile systems, traditionally reinforced coupling beams, containing longitudinal steel and closed hoops, are only permitted if the shear is low and if the span-to-depth ratio is relatively large. Diagonally reinforced coupling beams are required if the shear is high due to their excellent ductility and energy absorbing capability. The diagonal reinforcement is not practical if the span-to-depth ratio is greater than about 2.

Specimens 1 and 2 were constructed and tested to investigate the feasibility of using steel link beams in reinforced concrete coupled wall systems. These specimens had span-to-depth ratios of 3.4, significantly larger than the practical limit for diagonally reinforced coupling beams.

Two of the specimens tested by Shiu et al. (1978) are representative of the response of traditionally reinforced and diagonally reinforced concrete coupling beams having a span-to-depth ratio of 2.5. If the prototype structure considered in this research programme (see Chapter 2) had reinforced concrete coupling beams, these beams would have had a span-to-depth ratio of about 2.5. The hysteretic responses of the reinforced concrete coupling beams, tested by Shiu et al., are shown in Fig 1.4.

Figure 7.1 shows the equivalent elastic damping coefficient, β, for Specimens 1 and 2 and for those tested by Shiu. Both steel link beam specimens exhibited greater energy absorption

than the diagonally reinforced concrete member and far greater energy absorption than the traditionally reinforced concrete member. Specimen 2 exhibited the largest levels of hysteretic damping, with the least amount of decay with cycling.

7.2 Comparisons with Steel Link Beams in Eccentrically Braced Frames

The response of a representative steel link beam in an eccentrically braced frame (EBF) was chosen from the work of Engelhardt and Popov (1989). The link beam chosen had similar

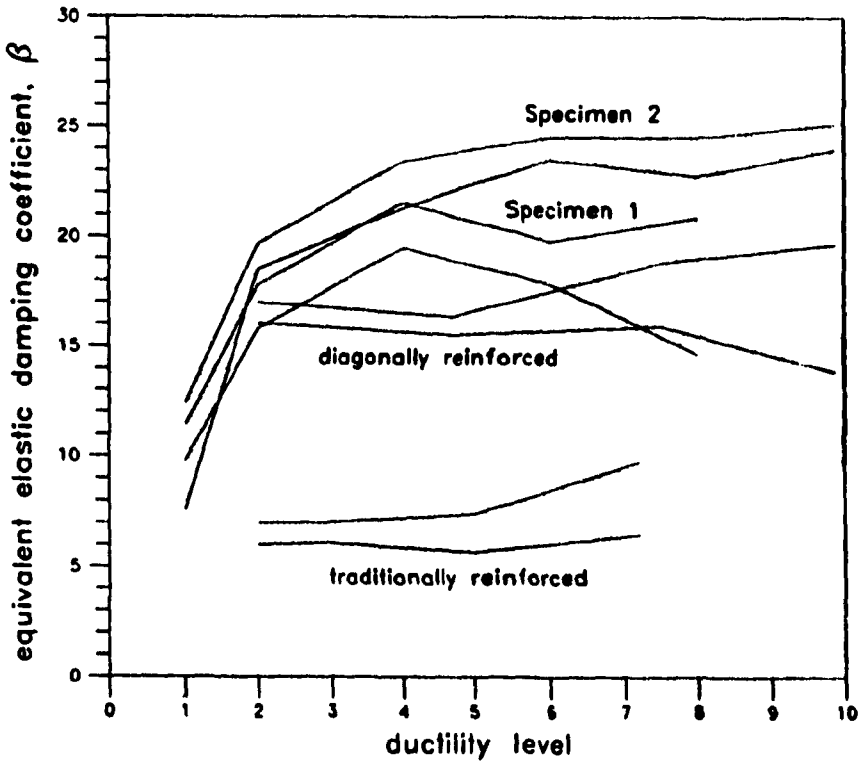

Figure 7.1 Equivalent elastic damping coefficients for Specimens 1 and 2 and reinforced concrete coupling beams tested by Shiu et al. (1978)

dimensions to those of Specimens 1 and 2 and a similar span-to-depth ratio (3.7 versus 3.4).

Figure 7.2 shows the excellent hysteretic behaviour of the steel link beam in an EBF, tested by Engelhardt and Popov. The ductilities achieved in Specimens 1 and 2 are comparable to those achieved by well-detailed link beams in EBFs. Figure 7.3 shows the equivalent damping coefficient, β, determined from this hysteretic response and those of Specimens 1 and 2. The

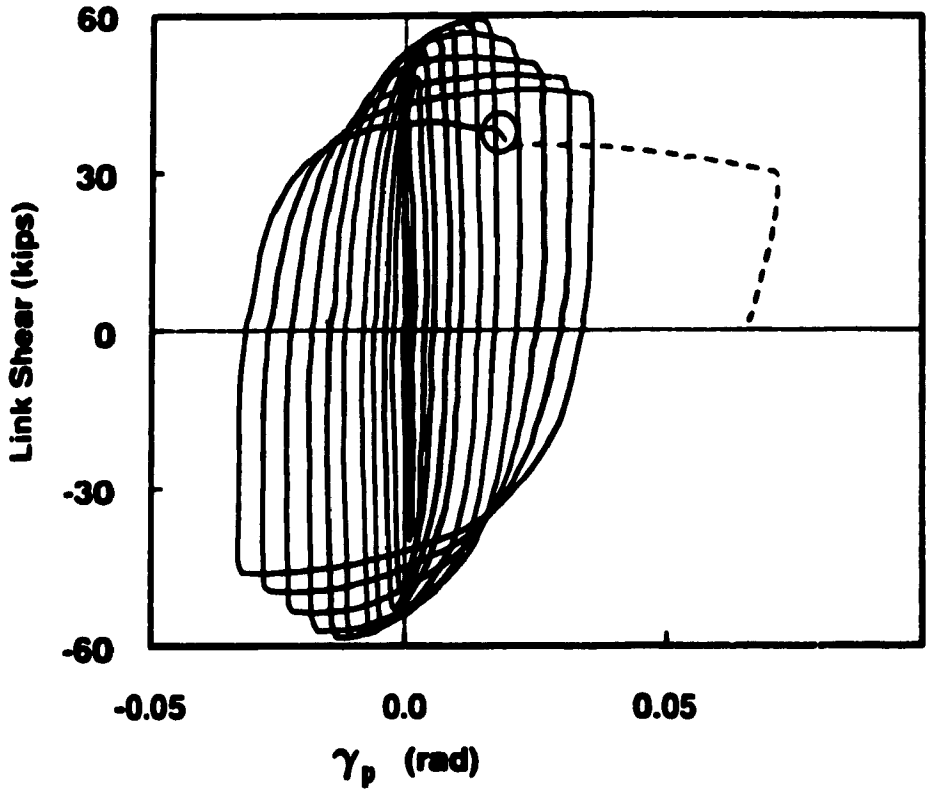

Figure 7.2 Shear versus link beam rotation in an eccentrically braced frame tested by Engelhardt and Popov (1989)

tests performed by Engelhardt and Popov had only one cycle at each load level and no significant decay occurred between the positive and negative half cycles at each displacement level.

It can be seen from Fig. 7.3 that the equivalent elastic damping coefficient for Specimen 2 is comparable to that of the link beam in an EBF, and above that exhibited by Specimen 1. These comparisons indicate that the refinements to the design of the embedment, in Specimen 2, have been sufficient to keep the embedded steel member and the embedment region elastic. The behaviour of Specimen 2 demonstrates the ability of steel link beams coupling reinforced concrete walls to provide energy absorption levels and ductilities similar to those provided by steel link beams in eccentrically braced frames.

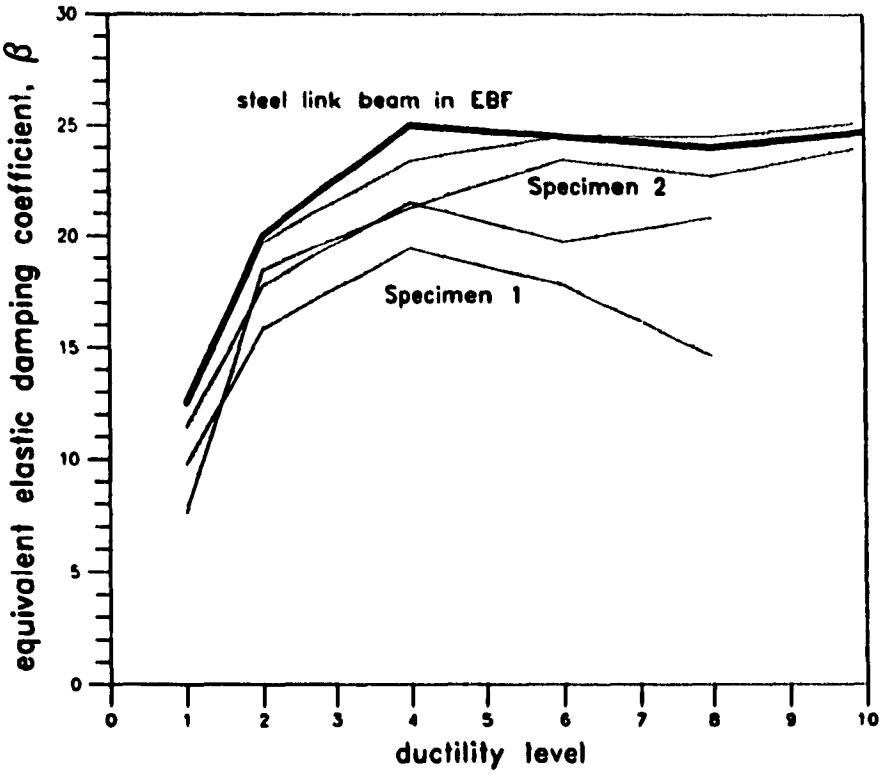

Figure 7.3 Equivalent elastic damping coefficients for Specimens 1 and 2 and a steel link beam in an eccentrically braced frame tested by Engelhardt and Popov (1989)

Chapter 8
Conclusions and Design Recommendations

In recent years, researchers have investigated novel approaches for improving the ductility and energy absorption of reinforced concrete coupling beams in ductile flexural wall systems. For span-to-depth ratios less than about 2, specially detailed diagonal reinforcement (e.g., Paulay and Binney, 1974) has been shown to significantly improve the reversed cyclic loading response. The objective of this research programme is to investigate the feasibility of using structural steel members, having their ends embedded in the walls, to replace reinforced concrete coupling beams. Two full-scale, test specimens were designed and tested, in reversed cyclic loading, in order to investigate the response of this new type of construction.

The results of this experimental programme have shown that it is possible to achieve excellent ductility and energy absorption characteristics by carefully designing and detailing the steel link beams and the reinforced concrete embedment regions.

For link beams having small to medium span-to-depth ratios, excellent response, similar to that exhibited by link beams in eccentrically braced frames can be achieved if the following design and detailing requirements are met:

i. The clear span of the link beam is designed and detailed to remain elastic in flexure while attaining its ultimate capacity in shear according to plastic design requirements.

ii. The web in the clear span is detailed such that it can develop large shear deformations beyond yielding. As such, the web is chosen to conform with the requirements for a Class 1 section and is adequately stiffened to prevent web and flange instabilities.

iii. In calculating the effective clear span for design purposes, the effect of the spalling of the cover concrete at the inside face of the wall is taken into account.

iv. Additional stiffeners are provided inside the embedment region, in the region of expected cover spalling.

Although good link beam response was obtained using these design criteria, it was found that even greater ductilities and energy absorption were attained if the web of the link beam in the embedment region was strengthened in such a way as to assure that the embedded region of the link beam remained elastic in shear and flexure while the link beam clear span attained its ultimate shear capacity.

In order to ensure that the link beam may perform in the desired ductile manner, the reinforced concrete embedment region must be designed and detailed in the following manner:

i. The embedment must be designed for a shear and moment corresponding to the development of the full capacity of the link beam.

ii. A reduced embedment length must be considered in order to account for the effects of the cover spalling at the inside faces of the walls. This reduction in embedment should correspond to the increased clear span length used to determine the capacity of the link beam.

iii. Vertical reinforcing bars, placed near the inside face of the walls, must be sufficient to provide adequate control of the cracking along the link beam flange-concrete interface.

It is important to note that the flexural walls themselves must be designed to resist the probable resistances of the link beams. The design criteria proposed should be considered in addition to the ductile design and detailing of the individual walls comprising the system.

The use of prefabricated steel link beams embedded in reinforced concrete walls provides an excellent level of quality control for these critical structural elements. Furthermore, the use of embedded steel link beams greatly simplifies the formwork requirements for coupled walls and requires a significantly less complex erection procedure than traditionally or diagonally reinforced concrete coupling beams.

It is evident from this preliminary research programme that the use of steel link beams in reinforced concrete coupled wall systems is a feasible alternative to traditionally or diagonally reinforced concrete coupling beams. The superior performance of this novel structural system is well suited for structures designed for large levels of ductility. The relative simplicity of design and erection, however, make this type of system feasible for any coupled wall system.

8.1 Areas for Further Investigation

The encouraging results of this preliminary study suggest a number of possibilities for future investigations of steel link beams in reinforced concrete coupled wall systems. These include:

i. Investigations into link beams with larger span-to-depth ratios. Larger moment-to-shear ratios would be present in longer beams, the effect of these increased ratios on the design of the link beams needs to be investigated.

ii. Methods of providing mechanical connections of the link beam to the embedment concrete should be investigated. These would include 'drag bars' mounted to the embedded portion of the link beam or positive connection of the link beam to the vertical reinforcement at the inside face of the wall.

iii. A simpler approach for strengthening the web in the embedment region would be to provide a doubler plate, welded all around and plug welded to the original web (designed for the clear span). This method of stiffening the embedded web is simpler and more practical than the butt-welded composite web used in Specimen 2. The effect of the eccentricity introduced by the doubler plate in the embedment would have to be investigated.

iv. Tests need to be performed on steel link beams having lower levels of ductility (flexural hinging modes) in order to provide design and detailing guidance for structures designed with lower R values.

v. The degree of lateral support supplied by the wall embedment to the link beam should be investigated and compared to the recent lateral load recommendations proposed by Engelhardt and Popov (1989). Furthermore the degree of lateral support, if any, supplied by the presence of a floor slab should be investigated.

vi. The interaction of localised embedment forces, together with the level of axial load in the walls should be investigated.

vii. The possibility of using externally applied structural steel plates as a retrofit measure for existing reinforced concrete coupling beams should be investigated. Such an investigation would examine the response of a reinforced concrete coupling beam previously subjected to a number of load cycles at its service load level and then retrofitted with an external steel plate.

References

Associate Committee on the National Building Code, 1990, National Building Code of Canada 1990, National Research Council of Canada, Ottawa, Ont.

Associate Committee on the National Building Code, 1990, Supplement to the National Building Code of Canada 1990, National Research Council of Canada, Ottawa, Ont.

Canadian Institute of Steel Construction (CISC), 1985, Handbook of Steel Construction, CISC, Willowdale, Ont.

Canadian Portland Cement Association (CPCA), 1986, Concrete Design Handbook, CPCA, Ottawa, Ont.

Canadian Prestressed Concrete Institute (CPCI), 1987, Metric Design Manual, CPCI, Ottawa, Ont.

Prestressed Concrete Institute (PCI), 1985, PCI Design Handbook, PCI, Chicago, Ill.

SEAOC, 1988, Recommended Lateral Force Requirements, Seismology Committee, Structural Engineers Association of California (SEAOC).

Berg, V.B. and Stratta, J.L., 1964, Anchorage and the Alaska Earthquake of March 27, 1964, American Iron and Steel Institute, New York, 63 pp.

Bertero, V.V. and Popov, E.P., 1975, *Hysteretic behaviour of reinforced concrete flexural members with special web reinforcement*, Proceedings of U.S. National Conference on Earthquake Engineering, Ann Arbor, June 1975, pp 316-326.

Engelhardt, M.D. and Popov, E.P., 1989, Behaviour of Long Links in Eccentrically Braced Frames, Earthquake Engineering Research Center, Berkeley, Report No. UCB/EERC-89/01, 406 pp.

Fiorato, A.E. and Corley, W.G., 1977, *Laboratory tests of earthquake resistant structural wall systems and elements*, Workshop on Earthquake Resistant Reinforced Concrete Building Construction, vol. III, University of California, Berkeley, July 1977, pp 1397-1402.

Harries, K.A., Cook, W.D., Redwood, R.G. and Mitchell, D., 1992, *Concrete walls coupled by ductile steel link beams*, Proceedings of Tenth World Earthquake Engineering Conference, Madrid, July, 1992.

Hawkins, N., Mitchell, D. and Hanna, S., 1975, *The effects of shear reinforcement on the reversed cyclic loading behaviour of flat plate structures*, Canadian Journal of Civil Engineering, Vol. 2, No. 4, December 1975, pp 572-582.

Kasai, K. and Popov, E.P., 1986, A Study of Seismically Resistant Eccentrically Braced Frames, Earthquake Engineering Research Center, Berkeley, Report No. UCB/EERC-86/01, 215 pp.

MacLeod, I.A., 1966, Lateral Stiffness of Shear Walls with Openings in Tall Buildings, Pergamon Press, Oxford pp 142-162.

Malley, J.O. and Popov, E.P., 1983a, Design of Links and Beam to Column Connections for Eccentrically Braced Steel Frames, Earthquake Engineering Research Center, Berkeley, Report No. UCB/EERC-83/03, 62 pp.

Malley, J.O. and Popov, E.P., 1983b, Design Considerations for Shear Links in Eccentrically Braced Frames, Earthquake Engineering Research Center, Berkeley, Report No. UCB/EERC-83/24, 117 pp.

Marcakis, C. and Mitchell, D., 1980, *Precast concrete connections with embedded steel members*, PCI Journal, Vol. 25, No. 4, July/August 1980, pp 88-116.

Mitchell, D. and Cook, W.D., 1989, Testing of Half-Scale Reinforced Concrete Link Beam - Bell Canada Office Building, 160 Elgin Street, Ottawa, Internal report prepared for Mr. R. Slattery, Houser, Henry, Louden and Syron, Toronto. 19pp.

Paparoni, M., 1972, *Model studies of coupling beams*, Proceedings of the International Conference on Tall Concrete and Masonry Buildings, August, 1972, Vol. 3, pp 671-681.

Park, R. and Paulay, T., 1975, Reinforced Concrete Structures, John Wiley and Sons, New York. (Chapter 12 - Shear Walls of Multistory Buildings.)

Paulay, T., 1969, The Coupling of shear walls, Volumes 1 and 2, (doctoral thesis, University of Canterbury, New Zealand). 432 pp.

Paulay, T., 1971, *Simulated seismic loading of spandrel beams*, Journal of Structural Division, ASCE, Vol 97, ST9, September, 1971, pp 2407-2419.

Paulay, T. and Binney, J.R., 1974, *Diagonally reinforced coupling beams of shear walls*, Shear in Reinforced Concrete, Special Publication No. SP-42, American Concrete Institute, Detroit. pp 579-598.

Paulay, T., 1976, *Ductility of reinforced concrete shearwalls for seismic areas*, Reinforced Concrete Structures in Seismic Zones, Special Publication No. SP-53, American Concrete Institute, Detroit. pp 127-147.

Paulay, T., 1986, *The design of ductile reinforced concrete structural walls for earthquake resistance*, Earthquake Spectra, Vol. 2, No. 4, 1986, pp 783-823.

Reoder, C.W. and Popov, E.P., 1978, *Eccentrically braced steel frames for earthquakes*, Journal of the Structural Division, ASCE, Vol. 104, No. ST3, March 1978, pp 391-411.

Rosman, R., 1964, *Approximate analysis of shear walls subject to lateral loads*, American Concrete Institute Journal, Vol. 61, No. 6, June 1964, pp 717-732.

Santhakumar, A.R., 1974, Ductility of coupled shear walls, (doctoral thesis, University of Canterbury, New Zealand). 385 pp.

Schwaighofer, J. and Microys, H.F., 1970, Analysis of Shear Wall Structures using Standard Computer Programs

Shiu, K.N., Barney, G.B., Florato, A.E. and Corley, W.G., 1978, *Reversed load tests of reinforced concrete coupling beams*, Central American Conference on Earthquake Engineering, El Salvador, January 1978, pp 239-249.

Stafford-Smith, B. and Coull, A., 1991 Tall Building Structures, John Wiley and Sons, 537 pp.

Subedi, N.K., 1989, *Reinforced concrete beams with plate reinforcement for shear*, Proceedings of the Institution of Civil Engineers (Great Britain), Part 2, Vol. 87, September 1989, pp 377-399.

Appendix A

Design and Analysis of Test Specimens

Appendix A.1 - Design of Steel Link Beam with Specified Material Properties

Trial section:

Flange: 134 x 18 mm
Web: 5 mm thick
Overall Height: 350 mm
F_y = 300 MPa

Clause numbers refer to CAN/CSA S16.1-M89.

Verification: Class of Section

$$\frac{b}{2t} = \frac{134}{36} = 3.72 < \frac{145}{\sqrt{F_y}} = 8.37 \quad \textit{Class 1} \qquad \text{§11.1.1}$$

$$\frac{h}{w} = \frac{(350-36)}{5} = 62.8 < \frac{1100}{\sqrt{F_y}} = 63.5 \quad \textit{Class 1} \qquad \text{§11.1.1}$$

Bending resistance:

$$\begin{aligned} M_r &= (0.25(5)(314)^2 + 134(18)(350-18))0.3x10^{-3} \\ &= (123245 + 800784)0.3x10^{-3} \\ &= 277.2\ kNm \end{aligned} \qquad \text{§13.5}$$

but the web should be ignored because it is yielding in shear:

$$\begin{aligned} \therefore M_r &= (800784)0.3x10^{-3} \\ &= 240.2\ kNm \end{aligned} \qquad \text{§D2}$$

Shear resistance:

$$\begin{aligned} V_r &= 0.55A_wF_y \\ &= 0.55(350)(5)(0.300) \\ &= 289\ kN \end{aligned} \qquad \text{§13.4.2}$$

including the effect of strain hardening:

$$\begin{aligned} V_r &= 0.70A_wF_y \\ &= 0.70(350)(5)(0.300) \\ &= 368\ kN \end{aligned}$$

assuming a clear span of 1200 mm:

	V (kN)	M (kN•m)	M_r (kN•m)
Theoretical shear yield load	289	173	240
Probable maximum shear load	368	221	240

Web stiffeners:

full depth: at ends, t = 10 mm
distance from ends: 600 mm

Intermediate:

$$spacing \le 38w - 0.2d$$
$$= 38(5) - 0.2(350)$$
$$= 120\ mm$$

§D8(a)

all one sided stiffener plates:

$$width > \frac{134}{2} - 5 = 62\ mm\ ,\ say\ 65 x 10\ mm$$

§D9

weld to web: weld must transfer:

$$A_s F_y = 195\ kN$$

§D10

use a 5 mm weld on one side:

$$V_r = 0.765(322) = 247\ kN > 195\ kN \ldots . OK$$

§13.13.1

weld to flanges: capacity of each end:

$$0.25 A_s F_y = 49\ kN$$

§D10

length of 5 mm weld required:

$$length > \frac{49}{0.765} = 64\ mm$$

use a 5 mm weld full length on one side.

Ends:

$$\frac{h_w}{t_w} = \frac{314}{5} = 62.8 \quad < \quad \frac{1100}{\sqrt{F_y}} = 63.5$$

§11.1.1

therefore stiffeners are not required.

Web to flange welds:

must develop yield stress of web:

$$\omega 0.67 F_y = say,\ 1\ kN/mm$$

§13.13.1

2 - 5 mm welds have capacity:

$$2(5)(153)(10^{-3}) = 1.53\ kN/mm \ldots . OK$$

Unsupported length

Clause 27.2.2.1.(b) requires:

$$L_u = \frac{960 r_y}{\sqrt{F_y}} = \frac{960 \times 33.96}{\sqrt{300}} = 1922.8\,mm > 1200\,mm....OK \qquad \text{§13.7}$$

Web in embedded region of Specimen 2: required to remain elastic

Consider that the moment capacity is reached:

$$V_f = \frac{M_r}{\frac{l}{2}} = \frac{277.2}{\frac{1200}{2}} = 461.7\,kN$$

solving for the required web thickness:

$$t_w = \frac{V_r}{0.55 h F_y} = \frac{461.6}{0.55 \times 350 \times 0.300} = 7.99\,mm \qquad \text{§13.4.2}$$

choose an 8 mm web size inside the joint region.

Clearspan web to joint web weld: consider a full depth double bevel groove weld.

The joint resistance is the smaller of:

$$V_r = 0.67 \phi F_y A_m = 0.67 \times 0.9 \times 0.300 \times 350 \times 5 = 316\,kN \text{ or,} \qquad \text{§13.13.1}$$
$$V_r = 0.67 \phi_w X_u A_w = 0.67 \times 0.67 \times 0.480 \times 310 \times 5 = 334\,kN$$

therefore, a full depth double bevel groove weld, butt welding the 5 mm and 8 mm web plates will be sufficient to carry the shear of 289 kN.

Appendix A.2 - Analysis of Link Beams with Actual Material Properties

Specimen 1

F_y of flange = 372 MPa
F_y of web = 320 MPa
d = 350 mm
b = 135 mm
t_f = 19.7 mm
t_w = 5.0 mm

Flexural resistance (excluding web)

$$M_r = (bt_f(d - t_f))F_y = 135x19.7x(350 - 19.7)x0.372x10^{-3} = 326.7\,kNm$$

considering the nominal value of F_y = 300 MPa:

$$M_r = (bt_f(d - t_f))F_{ym} = 135x19.7x(350 - 19.7)x0.300x10^{-3} = 263.4\,kNm$$

Shear resistance

$$V_r = 0.55A_wF_y = 0.55x350x5x0.320 = 308\,kN$$

Shear resistance including strain hardening effect

$$V_r = 0.7A_wF_y = 0.7x350x5x0.320 = 392\,kN$$

	V (kN)	M (kN•m)	M_r (kN•m)
Shear Yield	308	185	263
Shear Maximum	392	235	263

Specimen 2

F_y of flange = 295 MPa
F_y of web = 309 MPa
F_y of joint wed = 276 MPa
d = 345 mm
b = 135 mm
t_f = 19.2 mm
t_w = 4.7 mm
t_{wj} = 8.1 mm

Flexural resistance (excluding web)

$$M_r = (bt_f(d - t_f))F_y = 135x19.2x(345 - 19.2)x0.295x10^{-3} = 249.1\,kNm$$

Shear resistance

$$V_r = 0.55A_wF_y = 0.55x345x4.7x0.309 = 275\,kN$$

Shear resistance including strain hardening effect

$$V_r = 0.7A_wF_y = 0.7x345x4.7x0.309 = 350\,kN$$

Shear resistance of embedded link beam

$$V_r = 0.55A_wF_y = 0.55x345x8x0.276 = 419\,kN$$

	V (kN)	M (kN•m)	M_r (kN•m)
Web Shear Yield	275	165	249
Web Shear Ultimate	350	210	249
Joint Shear Yield	419	251	249

Appendix A.3 - Design of Reinforced Concrete Embedment Regions

Specimen 1

l = 600 mm
l_e = 600 mm
bearing width = 135 mm
centre to centre of ties = 208 mm
f_c' = 26 MPa

Embedment capacity: (according to Mitchell and Marcakis, 1990)

$$\textit{Lever arm} = e = l + \frac{l_e}{2} = 600 + \frac{600}{2} = 900\ mm$$

Note that this eccentricity does not account for the effects of cover spalling

Capacity of concrete embedment region:

$$V_e = \frac{0.85 f_c' b l_e}{1 + 3.6\frac{e}{l_e}} = \frac{0.85 \times 26 \times 208 \times 600}{1 + 3.6 \times \frac{900}{600}} = 430\ kN$$

Required Capacity:

Expected shear yield = 308 kN ..... OK
Expected maximum shear = 392 kN ..... OK

Specimen 2

l = 640 mm
l_e = 560 mm
c = 40 mm
bearing width = 135 mm
centre to centre of ties = 208 mm
f_c' = 43 MPa

Embedment capacity: (according to Mitchell and Marcakis, 1980)

$$\textit{Lever arm} = e = l + \frac{l_e}{2} + c = 640 + \frac{560}{2} + 40 = 920\ mm$$

Note that this eccentricity does account for the effects of cover spalling

Capacity of concrete embedment region:

$$V_c = \frac{0.85 f_c' b l_e}{1 + 3.6\frac{e}{l_e}} = \frac{0.85 x 43 x 208 x 560}{1 + 3.6 x \frac{920}{560}} = 616\ kN$$

Required Capacity:

Expected shear yield = 295 kN ..... OK
Expected maximum shear = 375 kN ..... OK

Appendix B

Summary of Loads and Deflections at the Peak Load Stages

Specimen 1

Loadstep	Data Time	Load (kN)	Vertical (mm)	Horiz. (mm)	Notes
1A	214 11:50:13	+100.17	+1.91	0	
1B	214 12:53:08	-101.21	-2.06	0	
2A	214 13:47:18	+100.90	+2.01	0	
2B	214 14:05:37	-98.32	-2.35	0	
3A	214 14:25:09	+98.34	+1.98	0	
3B	214 14:51:45	-101.40	-2.30	0	
4A	214 15:19:47	+197.99	+4.65	0	first crack at beam top flange
4B	214 15:55:06	-199.40	-4.56	0	first crack at beam bottom flange
5A	217 09:30:17	+195.97	+4.61	0	
5B	217 10:02:06	-197.97	-4.78	0	
6A	217 10:19:26	+198.39	+4.63	0	
6B	217 10:42:12	-198.02	-4.76	0	
7A	217 11:27:20	+249.33	+6.75	0	first local yielding of beam web
7B	217 12:06:16	-249.54	-6.13	0	
8A	217 13:52:33	+251.41	+6.86	0	
8B	217 14:08:26	-247.39	-6.54	0	
9A	217 14:17:41	+246.91	+6.77	0	
9B	217 14:36:14	-250.95	-6.91	0	
10A	217 15:27:13	+303.31	+12.01	0	general yield in beam web; first spalling
10B	217 16:39:26	-300.08	-11.08	0	
11A	218 09:38:18	+300.59	+11.44	0	
11B	218 10:28:01	-299.10	-11.59	0	front cover completely cracked
12A	218 11:05:15	+301.74	+11.47	0	
12B	218 11:24:12	-301.06	-10.82	0	
13A	218 12:59:12	+347.53	+24.46	2.67	crushing at both flanges
13B	218 13:57:50	-360.26	-24.76	3.86	crushing at both flanges
14A	218 15:15:51	+356.72	+24.17	6.53	
14B	218 15:45:45	-369.36	-26.14	7.44	
15A	218 16:08:26	+352.42	+25.11	10.06	crushing more severe
15B	218 16:46:09	-359.39	-27.43	11.73	
16A	219 10:32:36	+375.05	+46.78	15.82	
16B	219 11:46:06	-386.83	-50.10	17.27	first vertical crack 600 mm from face yield and
17A	219 14:05:05	+373.72	+50.06	20.23	bucking of web stiffeners
17B	219 14:44:49	-384.89	-48.26	21.89	tensile cracking at compressive strut
18A	221 09:55:19	+374.55	+49.29	24.74	install horizontal clamps
18B	221 11:17:27	-385.00	-49.35	27.00	
19A	225 11:41:00	+386.37	+70.34	30.76	notable bending in end web stiffeners
19B	225 14:52:06	-409.12	-75.51	31.29	
20A	226 10:02:49	+383.41	+69.92	36.78	
20B	226 10:52:17	-404.05	-76.01	36.30	
21A	226 13:40:53	+379.35	+69.94	43.36	front cover spalled off
21B	226 14:36:23	-396.03	-76.06	42.37	
22A	226 16:26:53	+387.67	+93.22	49.35	
22B	227 10:12:57	-398.92	-102.07	49.50	side cover spalling; twisting of beam
23A	227 12:24:47	+371.74	+93.50	57.40	further front cover spalling
23B	227 13:56:45	-373.13	-99.88	61.98	loss of confined concrete behind spalling
24A	227 15:51:00	+358.56	+95.24	67.31	side spalling restrained by vertical clamp
24B	227 16:50:16	-327.84	-100.56	69.85	no concrete around first rebars; first yield of rebars
END	228 all day	+344.27	+122.84		

Specimen 2

Longleter	Doric Time	Load (kN)	Vertical (mm)	Horiz. (mm)	Notes
1A	310 17:07:52	+100.12	+2.36	0	
1B	310 17:50:29	-99.18	-2.39	0	
2A	310 18:04:41	+99.66	+2.60	0	
2B	310 18:19:22	-101.32	-2.35	0	
3A	310 18:24:24	+99.95	+2.56	0	
3B	310 18:33:34	-93.61	-2.38	0	
4A	311 09:44:19	+199.93	+4.94	0	first crack at beam top flange
4B	311 11:12:17	-194.22	-4.59	0	first crack at beam bottom flange
5A	311 11:20:52	+199.81	+4.91	0	
5B	311 11:33:58	-199.21	-5.20	0	
6A	311 11:44:47	+198.16	+4.86	0	
6B	311 13:32:52	-195.40	-5.33	0	
7A	311 14:28:39	+273.94	+11.46	0	general yield in beam web
7B	311 15:30:59	-272.94	-9.16	0	
8A	311 15:53:37	+275.40	+10.99	0	first vertical cracking in both walls
8B	311 16:46:32	-273.75	-10.54	0	
9A	312 10:19:16	+273.55	+11.09	0	
9B	312 10:57:42	-274.62	-9.63	0	
10A	312 11:59:01	+311.82	+22.05	0	
10B	312 12:46:17	-332.99	-22.24	0	
11A	312 14:19:23	+324.35	+21.90	0	
11B	312 14:48:13	-336.53	-22.86	0	
12A	312 15:32:17	+325.45	+22.45	0	
12B	312 16:09:52	-336.87	-23.11	0	
13A	315 10:55:57	+358.48	+44.19	0	clear formation of tension cracks along struts
13B	315 12:16:47	-366.54	-44.53	3.27	
14A	315 14:39:54	+358.16	+43.96	0	
14B	315 14:59:50	-366.04	-44.18	4.83	
15A	315 16:05:17	+377.46	+44.09	1.86	
15B	315 16:36:32	-393.04	-45.43	6.17	
16A	316 11:03:39	+390.53	+65.97	3.32	spalling on face of East wall
16B	316 12:23:46	-429.00	-65.23	9.85	
17A	316 14:30:52	+401.62	+66.26	8.03	
17B	316 15:24:33	-426.96	-67.07	15.93	
18A	316 17:17:06	+400.51	+66.40	13.92	loss of side cover on East wall
18B	316 17:59:30	-427.81	-66.83	21.67	web buckling between all stiffeners
19A	317 11:45:53	+409.81	+66.01	22.76	
19B	317 12:51:01	-445.56	-90.34	33.02	
20A	317 15:40:07	+412.13	+66.01	33.02	
20B	317 16:52:26	-436.67	-66.83	42.44	
21A	318 11:44:34	+436.41	+66.16	45.29	both joint webs yielding
21B	318 15:57:41	-426.04	-66.79	56.52	yielding of web stiffeners
22A	319 11:50:30	-399.70	+110.64	55.83	
22B	319 13:17:22	-424.18	-110.29	71.96	
end	319 15:44:26	-361.31	-150.26		